Heliyon 10 (2024) e31434

Contents lists available at ScienceDirect

Heliyon

journal homepage: www.cell.com/heliyon

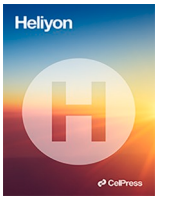

Research article

Biocompatible antibiotic-coupled nickel-titanium nanoparticles as a potential coating material for biomedical devices

Sarah McGlumphy [a,b], Aakriti Damai [a,b], Lena Salameh [a], Gabriell B. Corbin [b], Qiang Wang [c], John Markiewicz [a], Jennifer J. Mosher [b], Nadja Spitzer [b,**], Rosalynn Quiñones [a,*]

[a] Department of Chemistry, Marshall University, Huntington, WV, 25755, USA
[b] Department of Biological Sciences, Marshall University, Huntington, WV, 25755, USA
[c] Shared Research Facilities, West Virginia University, Morgantown, WV, 25606, USA

ARTICLE INFO

Keywords:
Nanoparticles
Neural differentiation
Phosphonic acid
Nitinol
Vancomycin
Ceftriaxone
Metallic implants
Biocompatibility
Antibacterial activity

ABSTRACT

The challenges facing metallic implants for reconstructive surgery include the leaching of toxic metal ions, a mismatch in elastic modulus between the implant and the treated tissue, and the risk of infection. These problems can be addressed by passivating the metal surface with an organic substrate and incorporating antibiotic molecules. Nitinol (NiTi), a nickel-titanium alloy, is used in devices for biomedical applications due to its shape memory and superelasticity. However, unmodified NiTi carries a risk of localized nickel toxicity and inadequately supports angiogenesis or neuroregeneration due to limited cell adhesion, poor biomineralization, and little antibacterial activity. To address these challenges, NiTi nanoparticles were modified using self-assembled phosphonic acid monolayers and functionalized with the antibiotics ceftriaxone and vancomycin via the formation of an amide. Surface modifications were monitored to confirm that phosphonic acid modifications were present on NiTi nanoparticles and 100% of the samples formed ordered films. Modifications were stable for more than a year. Elemental composition showed the presence of nickel, titanium, and phosphorus (1.9% for each sample) after surface modifications. Dynamic light scattering analysis suggested some agglomeration in solution. However, scanning electron microscopy coupled with energy-dispersive X-ray spectroscopy confirmed a particle size distribution of $<$100 nm, the even distribution of nanoparticles on coverslips, and elemental composition before and after cell culture. B35 neuroblastoma cells exhibited no inhibition of survival and extended neurites of approximately 100 μm in total length when cultured on coverslips coated with only poly-L-lysine or with phosphonic acid-modified NiTi, indicating high biocompatibility. The ability to support neural cell growth and differentiation makes modified NiTi nanoparticles a promising coating for surfaces in metallic bone and nerve implants. NiTi nanoparticles functionalized with ceftriaxone inhibited *Escherichia coli* and *Serratia marcescens (SM6)* at doses of 375 and 750 μg whereas the growth of *Bacillus subtilis* was inhibited by a dose of only 37.5 μg. NiTi-vancomycin was effective against *B. subtilis* at all doses even after mammalian cell culture. These are common bacteria associated with infected implants, further supporting the potential use of functionalized NiTi in coating reconstructive implants.

* Corresponding author.
** Corresponding author.
E-mail addresses: spitzern@marshall.edu (N. Spitzer), quinonesr@marshall.edu (R. Quiñones).

https://doi.org/10.1016/j.heliyon.2024.e31434
Received 18 February 2024; Received in revised form 4 May 2024; Accepted 15 May 2024
Available online 18 May 2024

1. Introduction

Metal osteopathic implants are used to repair bone injuries, especially those resulting from osteoarthritis and osteoporosis [1]. Stainless steel was one of the first alloys used in the biomedical industry because it has good corrosion resistance, but it has a high, potentially toxic, nickel and chromium content [2–4]. Alternatively, titanium implants are hampered by limited osseointegration and nerve regeneration at the injured site [5]. Surface films applied to metal implants effectively minimize corrosion and possible leaching of nickel ions [2,3,6–8]. Furthermore, surface roughness and nanoscale topography provided by nanoparticle coatings can promote cellular adhesion and biocompatibility [5,9–11].

Nitinol nanoparticles (NiTi), composed of nickel and titanium, were initially utilized in the aerospace industry to resist heat and fatigue in missile nose cones [12]. NiTi has low toxicity, corrosion resistance, superelasticity, and biocompatibility, making them promising candidates for coatings on reconstructive surgery implants [13,14]. A NiTi surface coating also has a high potential for additional biomedical applications in stents, equipment and tools, staples, and dental wires [3,4,15–23]. Passivation of the surface oxide layer on NiTi is a method to counteract the high reactivity of titanium, thereby minimizing corrosion and the release of nickel ions [24–31]. Although nickel ions have been reported to create a hypoxia-mimicking microenvironment that facilitates blood vessel regeneration [32], nickel is also highly reactive and potentially carcinogenic [33]. By limiting oxidation-reduction reactions between nickel and titanium via the formation of self-assembled monolayers (SAMs) on the NiTi surface, the toxicity of nickel in NiTi can be mitigated [34,35].

Phosphonic acids form a stable, protective layer over NiTi nanoparticles by forming a covalent phosphonate ester bond with the oxide layer naturally present on this material [8,26,34–37]. Phosphonic acids are an ideal choice to stabilize the NiTi surface due to their low p*K*a value and high stability when associated with metals [4]. The overall stability of NiTi was improved by modifying NiTi with octadecylphosphonic acid (ODPA), 16-phosphonohexadecanoic acid (COOHPA), and 12-aminododecylphosphonic acid (12-NH_2PA) [34]. Phosphonic acids containing a carboxylic acid tail group (COOHPA) introduce an electronegative terminal group, thus promoting biocompatibility [34,35,37]. NiTi modified with phosphonic acids carrying amino tail groups (12-NH_2PA) also have moderate wettability and provide a positively charged surface [34,38]. The phosphonic acid monolayer on the nanoparticle surface minimizes nickel toxicity, offers a biocompatible surface, and serves as a platform for attaching drugs or functional molecules, immobilizing them irreversibly.

Two drugs of interest in this study were the antibiotics vancomycin and ceftriaxone.. Vancomycin is commonly used against multidrug-resistant *Staphylococcus* infections [7,39,40] whereas ceftriaxone is a third-generation β-lactam drug targeting Gram-positive bacteria [41–43]. Ceftriaxone has one primary amino group whereas vancomycin has both primary and secondary amino groups (Fig. 1). Both antibiotics have amines that allow for simple surface-active molecules to be formed by linkage reactions with *N*-hydroxysuccinimide (NHS) and 1-ethyl-3-(3-dimethylaminopropyl)carbodiimide hydrochloride (EDC) [7,40,41,44]. Antimicrobial coupling has been successful with several nanomaterials including carbon nanotubes [45], calcium aluminum oxide [40], and nanosilver [46], but to our knowledge, this has not yet been reported for NiTi, a potentially superior biomimetic and biocompatible substrate.

NiTi nanoparticles were modified with phosphonic acid films, functionalized with two antibiotics (ceftriaxone or vancomycin), and extensively characterized. This study is the first to modify NiTi with organic films that were functionalized with antibiotics to explore the capabilities of a potential bioactive NiTi coating. To confirm the surface modifications, all NiTi samples were analyzed by spectroscopic techniques. In addition to measuring the hydrodynamic diameter of NiTi solutions, nickel, titanium, and phosphorus content

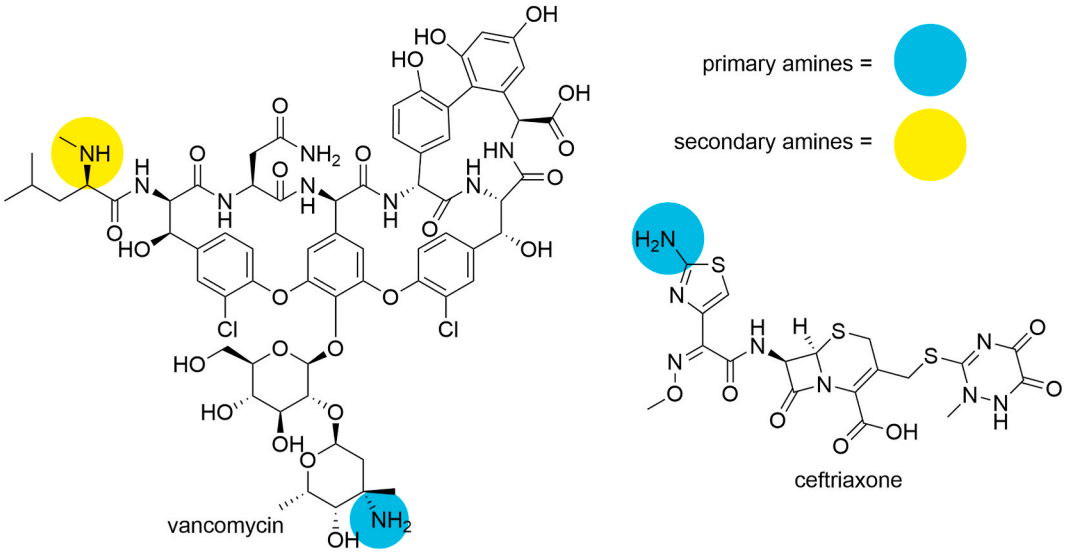

Fig. 1. Structure of Antibiotics used to modify NiTi nanoparticles with labeled amine.

was also determined.

Surfaces play an important role in how a cell interacts with its environment and SAM films can provide a polar organic interface between cells and the nanoparticles to promote adhesion [32,47–49]. Unmodified and modified NiTi were thus coated on poly-L-lysine-coated coverslips to test their efficacy in supporting neurite extension and survival of cultured rat B35 neuroblastoma cells, an established model of neuronal morphology and differentiation [50,51]. Upon differentiation in culture, B35 cells extend long neurites, a process that is essential to neurogenesis [50] and neuroregeneration [52]. Neurite extension depends on specific interactions between cellular ligands and the extracellular matrix, which must provide the cell with an appropriate terrain for adhesion, elongation, and wayfinding [52] to support growth and differentiation [53,54]. Normal survival and neurite extension by B35 cells grown on NiTi coatings suggest their high biocompatibility, and their potential efficacy in supporting neural regeneration on implants.

This work therefore confirms that NiTi nanoparticles, modified with phosphonic acid SAMs, are stable and supportive of mammalian cell adhesion and growth. Moreover, the SAMs provide ready chemical access for covalent linkage of other bioactive molecules on the NiTi surface, thereby offering myriad possibilities for biologically targeted functionalization of surface coatings.

2. Experimental DETAILS

2.1. Materials

NiTi nanoparticles (99.9% purity, 60–80 nm in diameter, Ni/Ti 50/50 atomic percent) were purchased from SkySpring Nanomaterials Incorporated. Octadecylphosphonic acid (ODPA), 97.0% purity, and 12-aminododecylphosphonic acid (12-NH_2PA), 95.0% purity, were purchased from Alfa Aesar. 16-phosphonohexadecanoic acid (COOHPA), 97% purity, nickel standard for ICP, 1000 ± 2 mg/L Ni in 3% nitric acid, phosphorus standard for ICP, 1001 ± 3 mg/L P in 3% nitric acid, titanium standard for ICP, 1000 ± 2 mg/L Ti in 3% nitric acid, Poly-L-lysine (poly-K) solution, NaH_2PO_4, and 4′,6-diamidino-2-phenylindole (DAPI) were purchased from Sigma Aldrich. Tetrahydrofuran (THF, Optima grade), Dulbecco's Modified Eagle Medium (DMEM), fetal bovine serum (FBS), Penicillin/Streptomycin (Pen/Strep), phalloidin-Alexa 568, Prolong Gold, trypsin, trypsin inhibitor, trypan blue, NaCl, paraformaldehyde (PFA), TritonX, bovine serum albumin (BSA), Live/Dead Assay Kit, round glass coverslips, concentrated nitric acid (TraceMetal grade), blank paper filter disks, 1-ethyl-3-(3 dimethylaminopropyl) carbodiimide hydrochloride (Pierce Premium-Grade EDC), Mueller-Hinton agar and broth were purchased from Fisher Scientific. Vancomycin hydrochloride, molecular biology grade was purchased from Thermo Scientific. 24-well tissue culture plates were purchased from Azer Scientific. Ceftriaxone Disodium Salt Hemiheptahydrate was purchased from TCI Chemicals. *N*-hydroxysuccinimide (NHS, 98+%) was purchased from Acros Organics. Ethanol (190 proof) was purchased from Pharmo-Aaper. Disodium phosphate (Na_2HPO_4) and potassium chloride (KCl) were purchased from AMRESCO. The rat B35 neuroblastoma cell line (ATCC #CRL-2754), *Escherichia coli* (ATCC #10798), and *Bacillus subtilis* (ATCC #6051) were purchased from ATCC. *Serratia marcescens* (SM6) was graciously donated by Dr. Lydia Bogomolnaya and *Staphylococcus epidermidis* (ATCC #12228) cultures were donated by Dr. Hongwei Wu. All chemicals in this study were used without further purification.

2.2. Nanoparticle modification

2.2.1. Phosphonic ester SAMs formation

To modify the nanoparticles, a 15 mM concentration of the ODPA, COOHPA, or 12-NH_2PA in 6 mL of THF were added to 0.35 g of NiTi nanopowder in 30 mL of THF as described previously [34]. Each solution was sonicated individually for 15 min. The solutions were sonicated together for another 30 min. The solutions were left under a hood to stir and dry for 24 h (Fig. 2, step 2). Next, ATR-IR scans of the unrinsed, modified NiTi were obtained. To remove unbound phosphonic acids, the samples were rinsed by sonication in 10 mL of THF, and vacuum centrifuged to separate the sample from THF [34]. ATR-IR spectroscopy was used again to monitor the extent to which the acids remained bonded to the surface of the NiTi. We previously reported that phosphonic acids remained chemically bound to the nanoparticles even after rinsing and vacuum centrifugation, indicating that the phosphonic acids are strongly attached to

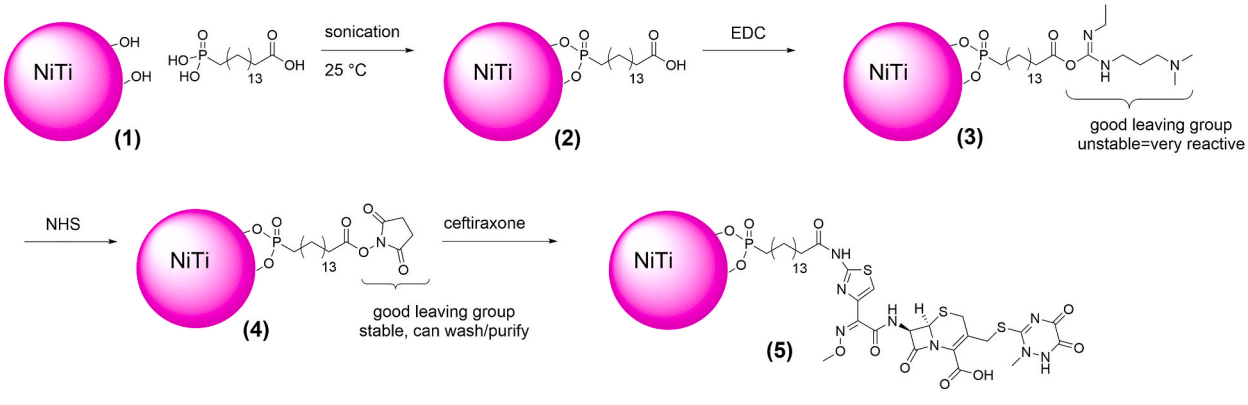

Fig. 2. Schematic of COOHPA on NiTi nanoparticles functionalized with ceftriaxone as an antibiotic.

the surface of the NiTi nanoparticles [34].

2.2.2. Antibiotic attachment

For antibiotic functionalization, only the NiTi-COOHPA from 2.2.1 was used because the carboxylic acid terminal group can be used to form an amide bond with the amines in the antibiotics (Fig. 2). Based on the moles of COOHPA used in the previous step, 2.4 equivalents of NHS and 2.4 equivalents of EDC were added to the sample, sonicated for 30 min, and allowed to stir for 1 h to form an activated NHS-ester *in situ* (Fig. 2, steps 3 and 4). Then, 2.4 equivalents of the antibiotic (ceftriaxone or vancomycin) dissolved in THF were added to the EDC/NHS and stirred overnight. The nanoparticles with covalently attached antibiotics (Fig. 2, step 5) were vortexed for 30 s with THF, vacuum centrifuged, and decanted. This rinsing procedure was repeated three times to remove byproducts of the reaction and unbound reagents.

2.3. Characterization of NiTi nanoparticles

2.3.1. ATR–IR

A Fourier transform infrared spectrometer (FT-IR, Thermo Scientific model Nicolet iS50, Waltham, MA) with a smart reflectance ATR accessory was used to collect the ATR-IR spectra. A germanium crystal was used. Backgrounds were obtained using unmodified NiTi nanoparticles, and 256 scans with a resolution of 4 cm^{-1} were collected. The ATR-IR spectra were used to confirm that the SAMs were bonded to the surface of the NiTi after rinsing with THF. ATR-IR spectra were also collected from samples after 18 months of storage under atmospheric conditions to show that the NiTi still had SAMs bonded to the surface.

2.3.2. ICP-OES

An inductively coupled plasma-optical emission spectrophotometer (ICP-OES, Agilent Technologies model 5110, Santa Clara, CA), equipped with a OneNeb nebulizer was used. The wavelengths for analysis were 216 nm for nickel, 334 nm for titanium, and 213 nm for phosphorus. The plasma conditions used were an generator power was 1200 W applied to the plasma, flow rates of 13 L $min^{-1}$for the plasma gas, and 1 L min^{-1} for the auxiliary gas flow rate with the nebulizer flow rate of 0.65 L min^{-1}. Each sample, blank, and standard were analyzed in triplicate. The data were analyzed using ICP Expert ICP-OES instrument software.

For metal oxide analysis, 7.5 mg of the NiTi nanoparticles were dissolved in 10 mL of concentrated nitric acid. The samples were stirred in a water bath for 35 min at 60–70 °C. Each sample was then quantitatively transferred to a 25-mL volumetric flask and diluted to the mark with deionized water. Standard solutions for nickel and titanium were prepared, consisting of 10–400 mg/L each, and standards for phosphorus were prepared from 0.1 to 20 mg/L. These solutions were made in a volumetric flask using 3% nitric acid. The detection limits calculated for nickel, titanium, and phosphorus were 5.6 ng/mL, 6.8 ng/mL, and 9.2 ng/mL respectively.

2.3.3. XPS

XPS measurements were performed using a scanning X-ray photoelectron spectrometer (ULVAC-PHI, Inc. Model PHI 5000 VersaProbe, Japan) at room temperature and under vacuum better than 10^{-6} Pa. All measurements were performed using a focused Al K-Alpha X-ray source at 1486 eV energy and 25 W power, with an X-ray spot size of 100 μm. The take-off angle of the photoelectron was set at 45^{o}. An analyzer pass energy of 117.4 eV and energy step of 0.5 eV were used for a survey scan, and high-resolution scans for nickel, titanium, oxygen, nitrogen, phosphorus, and carbon elements were carried out at an analyzer pass energy of 23.5 eV and energy step of 0.1 eV. The XPS spectra were referenced to the C1s peak at a binding energy of 284.8 eV.

2.3.4. DLS

A Zeta potential analyzer (Brookhaven model ZetaPlus, Holtsville, NY) was used to analyze the particle sizes of the NiTi nanoparticles by DLS in solutions of three different concentrations. These solutions of the NiTi nanoparticles were made in THF that was filtered three times using a syringe filter with a 0.2 μm pore size. NiTi nanoparticles at concentrations of 0.50, 0.75, and 1.0 mg/mL in THF were tested. Four measurements were taken for each solution. This was used to determine the most suitable concentration of NiTi nanoparticles for application to coverslips for cell culture (Section 2.4, below).

2.3.5. SEM/EDS

A scanning electron microscope (SEM, JEOL model JSM-7200 F, Japan) with a Zr01 W emitter electron source was used to observe the morphological characteristics of the nanoparticles coated on the coverslips. The sample data was collected at an acceleration voltage between 15 to 20 kV using the Lower Electron Detector (LED). The pressure was approximately 10^{-4} Pa with a working distance of 9–10 mm. Coverslips were attached with conductive tape to SEM stubs using gloves. Before imaging, samples were sputtered and coated with a thin layer of gold palladium.

For each site and magnification of SEM, elemental analysis was also conducted using Oxford Instruments Ultimax 100 with an X-max detector. Samples were analyzed using a probe current of 12 kV to keep the dead time less than 30% with a 4-min processing time. Data analysis was performed with Aztec 4.2 software. An elemental spectrum was collected for 20 s, while elemental mapping data was collected for 2 min.

2.4. B35 neuroblastoma cell culture, staining, and analysis

2.4.1. Preparation of coverslips with nanoparticles

Ultraclean sterile glass coverslips were coated with 100 μL 0.01% poly-L-lysine (poly-K) for 30 min or longer, washed with sterile deionized water, and allowed to dry. Unmodified and modified NiTi solutions were prepared at 0.75 mg/mL in THF and sonicated for 15 min as above. They were then kept on a rocker. NiTi solutions (bare NiTi, phosphonic-acid coated NiTi, or NiTi-COOHPA-antibiotic) were applied to poly-K-coated coverslips in two serial 50 μL aliquots (total 75 μg nanoparticles per coverslip) and allowed to dry between applications. Representative coverslips were imaged and analyzed with SEM to confirm that the nanoparticles were attached to the coverslips and homogeneously distributed.

In preparation for cell culture, coated coverslips were moved to individual wells of a 24-well culture plate and hydrated through an ethanol series of 70, 47, 28, 12, and 0% in distilled water. Coverslips were then washed twice with phosphate-buffered saline (PBS1: in mM: NaH_2PO_4, 2.69; Na_2HPO_4, 11.9; NaCl, 137; KCl, 27; pH7.4) and then incubated in fresh PBS1 at 37 °C and 5% CO_2 for 1 h. PBS1 was replaced with 450 μL Differentiation medium (DMEM, 1% Pen/Strep) and incubated at 37 °C and 5% CO_2 overnight.

2.4.2. Cell culture

Undifferentiated B35 cells were maintained in adherent culture in DMEM with 10% FBS and 1% Pen/Strep. Cultures were passaged with trypsin when they reached 80–90% confluence. For experimentation, cells were trypsinized, collected by centrifugation (Eppendorf Model 5702), and resuspended in a differentiation medium (no FBS). Cells were added to the medium on coated coverslips at a density of $4x10^4$ cells/well and allowed to differentiate at 37 °C in 5% CO_2 for 24 h (Thermo Forma Series II water-jacketed incubator, Model 3110).

After cell culture, some coverslips were washed thrice with PBS1 followed by 100 μL water. A sterile filter disk was used to collect the NiTi from the surface of the coverslip and placed on bacterial lawns for assessment of antimicrobial activity as below (section 2.5).

2.4.3. Phalloidin labeling for f-actin

The culture medium was removed, and B35 cells were washed with PBS1, followed by fixation for 15 min with fresh 4% PFA in PBS1. Coverslips were then washed with PBS2 (in mM: sodium phosphate, 100; NaCl, 150; pH7.4) and permeabilized for 10 min with 0.3% TritonX in PBS2). BSA (5%) in PBS2 was applied for 30 min as a blocking agent. Phalloidin-Alexa 568 (1:100) in block solution was then applied to stain F-actin for 20 min followed by five PBS2 washes and then DAPI in PBS2 (1:1000) for 5 min to stain nuclei. Coverslips were mounted on slides with ProLong Gold, left to cure overnight in the dark, and stored at 4 °C.

2.4.4. Live/dead assay

A working solution of 2 μM each ethidium homodimer-1 and calcein-AM was made fresh in PBS1. Cells pre-treated with 70% methanol in PBS1 for 30 min provided a positive control for dead label. Coverslips were washed twice with PBS1 and stained with 100 μL of working solution for 30 min at 37 °C in 5% CO_2. Coverslips were then mounted on slides with 10 μL PBS1, and images were immediately collected.

2.4.5. Imaging and analysis

Images were obtained with an epifluorescent inverted microscope (Leica model DM6000, Germany). For fixed cells stained with phalloidin-Alexa 568 and DAPI, single images were collected at 4 randomly selected fields of view from each coverslip. The total neurite length of two randomly selected cells was measured in each image using the NeuronJ plugin [55] in ImageJ (NIH) for a total of 8 cells per coverslip with which a mean total neurite length was calculated. The experiment was repeated with four coverslips for each NiTi solution.

For the live/dead assay, the automated stage and software on the microscope (Leica) were used to collect mosaic images of $\approx 8 \times 8$ mm from the center of each coverslip. The number of live and dead cells in each image were counted manually using the multi-point tool in ImageJ (mean 420 total cells per image). The experiment was repeated with three coverslips for each NiTi solution. And the proportion of live cells on coverslips coated with NiTi was normalized to the mean from coverslips coated with only poly-K.

Statistical analysis was performed using one-way ANOVA followed by Tukey's multiple comparisons. All statistical analyses and graphing were performed using GraphPad Prism.

2.5. Antimicrobial testing

The susceptibility of two classes of anti-bacterial drugs covalently bound to NiTi nanoparticles was tested by performing standard sensitivity tests to assess inhibition using sterile filter disks impregnated with unmodified or modified NiTi. For the 37.5 μg dose, sterile filter disks (which absorb 50 μL of fluid) were dipped in the 0.75 mg/mL NiTi solutions and allowed to dry. For the higher doses, 50 μL of the NiTi solutions were sequentially applied to poly-K coated coverslips and allowed to dry as described above until the reported dose was applied. The nanoparticle coating was then collected by scrubbing with a filter disk impregnated with 50 μL ethanol and allowed to dry. Bacterial cultures were grown overnight in Mueller-Hinton broth at 37 °C (Labnet 211DS Shaking incubator). Two Gram-positive bacterial strains, *Staphylococcus epidermidis* (ATCC 12228) [56] and *Bacillus subtilis* (ATCC 6051) [57] plus two Gram-negative strains, *Serratia marcescens* strain SM6 [58] and *Escherichia coli* (ATCC 10798) [59] were selected for this study.

100 μl of each bacterial culture (10^6-10^7) was spread on the Mueller-Hinton agar [60,61]. The disks containing each treatment were placed on the inoculated agar with sterile forceps and incubated for 18 h at 37 °C. Zones of inhibition (mm diameter) were measured

with a ruler to quantify the inhibition of bacterial growth by each NiTi preparation [62]. Statistical analysis was performed using one-way ANOVA followed by Tukey's multiple comparisons. All statistical analyses and graphing were performed using GraphPad Prism.

3. Results and DISCUSSION

3.1. Surface chemistry of functionalized NiTi

To examine the organization of the modifications on the NiTi surface in ATR-IR, the C–H stretches of the methylene group were used as reference peaks [34,37]. The values of ν_{CH2} after removal of the physically adsorbed films for nanoparticles modified with 12-NH_2PA, COOHPA, and ODPA were $\nu_{CH2\ asym}/\nu_{\ CH2\ sym}$ 2916 cm^{-1}/2847 cm^{-1}, 2916 cm^{-1}/2846 cm^{-1}, and 2915 cm^{-1}/2847 cm^{-1} respectively (Fig. 3). Previous findings support the results of the formation of these phosphonic films on NiTi nanoparticles [12]. To demonstrate that the organic acid films remained ordered and bound to the surface for the further surface reaction of COOHPA, ATR-IR analysis was performed after samples were modified more than 18 months prior. Infrared spectra indicated by the lack of change over time show that these films are strongly bound to the NiTi surface.

Functionalized carboxylic acid-terminated phosphonic acid (COOHPA) was used to immobilize two antibiotics onto NiTi nanoparticles as shown in Fig. 2. The NiTi surface was modified with COOHPA and characterized by ATR-IR, SS-NMR, SEM/EDS, and XPS as reported previously [34].

The carbonyl region of the IR spectra was analyzed. A peak at 1667 cm^{-1}, which corresponds to the $\nu_{C=O}$ of free carboxylic acid was observed, and it is accessible for further chemical reactions as shown in Fig. 4A. Furthermore, when compared to the unbound COOHPA, the carbonyl peak was observed at 1702 cm^{-1}. Then, the carboxyl group of COOHPA was transformed into an NHS-ester with EDC/NHS to form a good leaving group that was stable enough to be washed by solvent but also reactive enough to undergo further reactions with primary amines found in antibiotics (Fig. 1). This NHS-ester (Fig. 4B) was characterized by new IR peaks (1632 cm^{-1} and 1560 cm^{-1}). Later, when the antibiotics were added, a stable new amide bond was formed between the phosphonic acid film and the antibiotic (ceftriaxone or vancomycin). For ceftriaxone (Fig. 4C), IR peaks were observed at 1762 cm^{-1}, and 1602 cm^{-1}, which

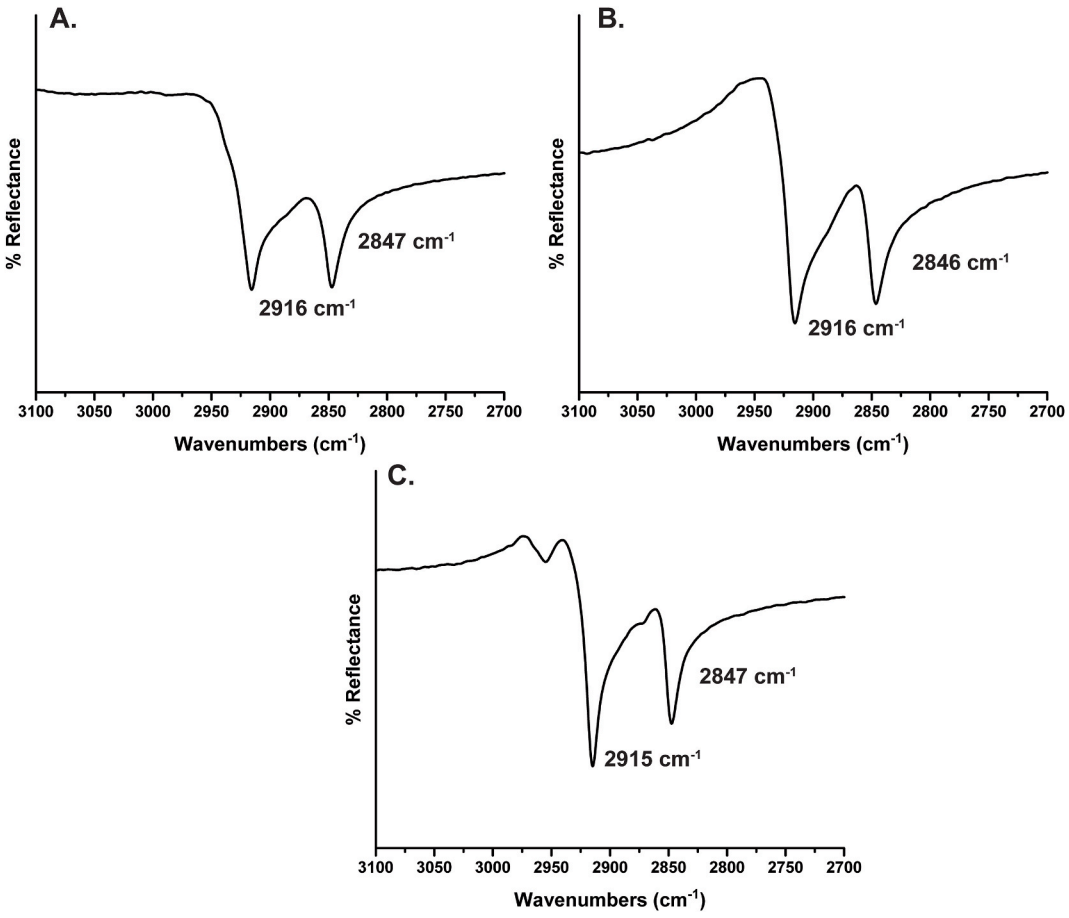

Fig. 3. Infrared spectra of CH region of NiTi nanoparticles modified with (A) 12-NH_2PA, (B) COOHPA, and (C) ODPA 18 months after preparation.

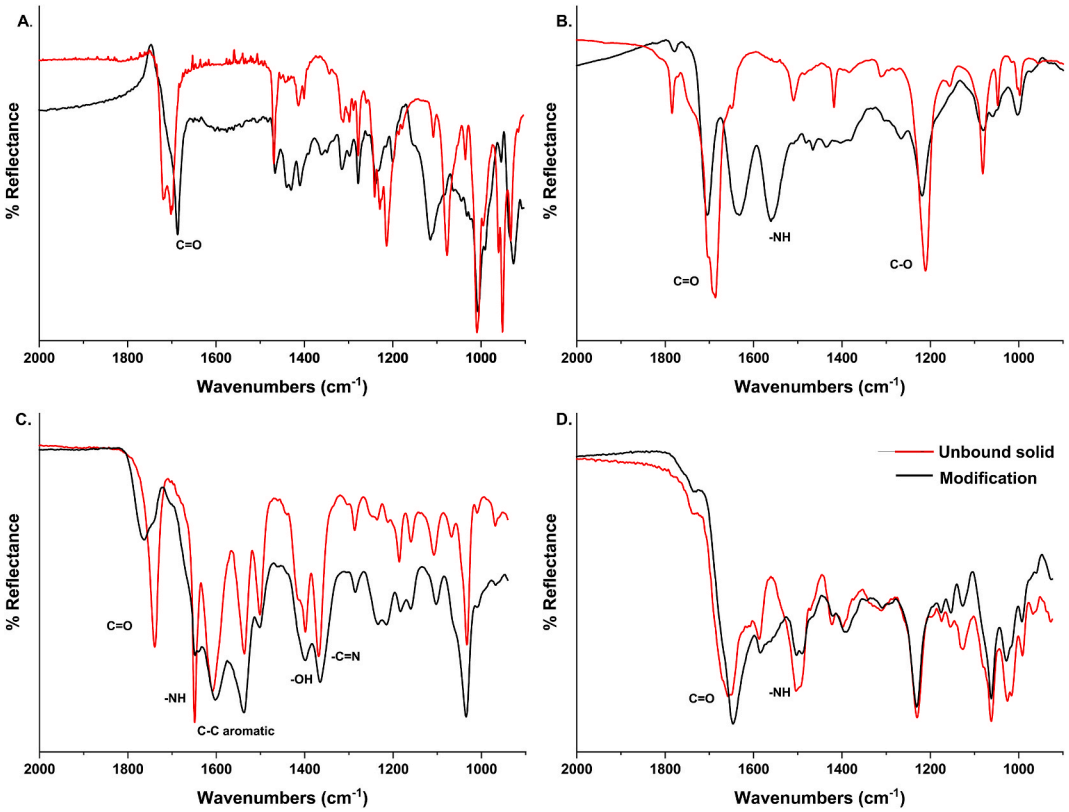

Fig. 4. IR spectra of the modifications (black spectra) steps for NiTi compared to unbound solid (red spectra): (A) IR of the carboxylic acid region of the carboxylic terminated phosphonic acid-modified sample (step 1), (B) EDC/NHS formation (step 2 and 3), (C) ceftriaxone attachment (step 4), an (D) vancomycin attachment. Both antibiotic samples were rinsed three times.

can be attributed to the amide (C=O and –NH) vibrations, and 1365 cm^{-1} is related to –C=N, and O–H vibrations as previously reported [42,43]. The peak at 1526 cm^{-1} is attributed to the aromatic ring vibrations [43]. The phosphonate vibration was observed at 1215 cm^{-1}, as previously reported of COOHPA bound on NiTi nanoparticles [34]. For vancomycin (Fig. 4D), IR peaks were observed at 1647, 1502 cm^{-1}, and 1390 cm^{-1}, which can be attributed to amide (C=O and –NH) formation as previously reported with other types of surface immobilizations on calcium surfaces [40]. It is noted that a peak at 1234 cm^{-1} can still be observed due to the phosphonate vibration from the head group of COOHPA film as previously reported [34].

3.2. Hydrodynamic diameter measurements

The average particle sizes of the NiTi nanoparticles in THF were obtained by the DLS as shown in Table 1. While DLS has not been shown to have sufficient size resolution to discriminate between agglomerates and does not always show a linear response to particle concentration, it was used as a screening tool to determine the best NiTi concentrations going forward in the project [63,64]. An increase in concentration from 0.50 to 1.0 mg/mL was correlated with an increase in particle size, suggesting agglomeration. The 0.5 mg/mL preparations had a high standard deviation and poor precision, indicating the possibility of a lack of homogeneity, which is consistent with a very diluted sample. Based on DLS analysis, a 0.75 mg/mL concentration was selected to continue with SEM-EDS and ICP-OES, mammalian cell culture, and antimicrobial testing.

Table 1
Particle size values of the hydrodynamic diameters of NiTi in THF in different concentrations obtained using dynamic light scattering (DLS).

Modifications	0.50 mg/mL	0.75 mg/mL	1.00 mg/mL
	Particle Size (nm)	Particle Size (nm)	Particle Size (nm)
COOHPA	193 ± 8	181 ± 5	211 ± 7
ODPA	177 ± 3	175 ± 11	182 ± 6
12-NH_2PA	179 ± 11	189 ± 18	195 ± 24
Ceftriaxone	210 ± 24	211 ± 18	227 ± 20
Vancomycin	229 ± 1	232 ± 8	269 ± 12

3.3. Nanoparticle composition on coverslips by ICP-OES

ICP-OES was used to quantify the concentration of nickel, titanium, and phosphorus in the nanoparticle solutions used to coat the poly-K-coated coverslips (0.75 mg/mL). Since the nanoparticles are black, the quantifications of the phosphonic acids and antibiotics on the surface of the nanoparticles would be inaccurate using a UV–Vis spectrometer. It was noted that the nanoparticles were difficult to dissolve in concentrated nitric acid. Temperature and time were optimized to promote maximal dissolution of the nanoparticles in nitric acid.

Table 2 shows ICP-OES results obtained from the NiTi nanoparticles dissolved in acid and the proportion of nickel, titanium, and phosphorus. The amounts calculated using a linear calibration curve of nickel and titanium were found to be higher on the unmodified samples of NiTi nanoparticles. As the samples were further modified with either phosphonic acid or antibiotics, the proportion of free or unbound nickel and titanium decreased. This trend was expected due to additional elements such as carbon, nitrogen, sulfur, and oxygen on the NiTi surface. Furthermore, others found that the leaching of nickel ions from NiTi alloy could have potential antibacterial effects [65]. Later, these samples were analyzed by SEM-EDS to confirm that the nanoparticles were adhered to the coverslips.

3.4. Confirming NiTi functionalization with antibiotics by XPS

The phosphonic acid coatings and attachment of antibiotics to the NiTi nanoparticles and their coverage on the poly-K coated coverslips were confirmed using XPS (Fig. 5). Compositional XPS survey scans (Fig. 5A) were taken with a pass energy of 117.4 eV and an energy step of 0.5 eV. The survey spectra for all samples display prominent Ti 2p and Ni 2p peaks, verifying the presence of NiTi nanoparticles. To highlight the effect of the COOHPA modification and antibiotic attachment, high-resolution P2p, S2p, and Cl2p spectra were also acquired from those samples, using a pass energy of 23.5 eV and an energy step of 0.1 eV, as shown in Fig. 5 (B-D). All samples modified with COOHPA exhibit clear P2p peaks, indicating the phosphorus from COOHPA (Fig. 5B). Moreover, a clear S2p signal was observed in the ceftriaxone-added samples (Fig. 5C), confirming the antibiotic's attachment to the NiTi nanoparticles. It was previously reported that S2p was a characteristic signal of ceftriaxone absorbate on a 2D nanosheet [66]. Similarly, Fig. 5D shows the Cl2p signal from the samples modified with vancomycin, further confirming the presence of the antibiotic. A previous report of vancomycin-coated magnetic nanoparticles also observed the characteristic Cl2p peak for vancomycin after grafting on their surface [67]. In addition to the spectral identifications outlined above, detailed peak fitting analysis further elucidates the binding energies associated with the observed phosphorus, sulfur, and chlorine signals. Specifically, the peak fitting suggests that the $P2p_{3/2}$ peak, associated with COOHPA, is located at a binding energy of 133.0 eV across all samples. In the case of the sulfur signal, the analysis indicates that the $S2p_{3/2}$ peak in the ceftriaxone-added samples is located at 163.8 eV. For vancomycin-modified samples, the peak fitting for the Cl2p spectrum identifies the $Cl2p_{3/2}$ peak at a binding energy of 197.7 eV.

To further quantify the XPS results obtained from the NiTi nanoparticles and their modifications, the atomic concentration ratios of the elements detected from each sample were calculated and are summarized in Table 3. In addition to the observation of sulfur in the ceftriaxone sample and chlorine in the vancomycin sample, there is also a clear enhancement of the carbon and nitrogen signals following the NHS/EDC treatment and antibiotic attachment. These findings are fully consistent with the reactions outlined in Fig. 2.

To verify the coverage of both unmodified and modified NiTi nanoparticles on poly-K coated coverslips, a bare poly-K coverslip, a coverslip coated with unmodified NiTi nanoparticles, and coverslips coated with 12-NH_2PA, COOHPA, or ODPA-modified NiTi particles were analyzed using XPS. The results are summarized in Fig. 6. Compositional survey scans (Fig. 6A) were conducted with a pass energy of 117.4 eV and an energy step of 0.5 eV. High-resolution Ni2p, Ti2p, and P2p spectra for the unmodified and phosphonic acid-modified samples were acquired using a pass energy of 23.5 eV and an energy step of 0.1 eV, as illustrated in Fig. 6 (B-D). Survey spectra for all coverslips coated with NiTi display Ti 2p and Ni 2p peaks, signifying the presence of NiTi nanoparticles. This is corroborated by the high-resolution spectra for Ni2p (Fig. 6B) and Ti2p (Fig. 6C). As previously noted by Refs. [34,68], distinct P2p peaks seen in Fig. 6D confirm the presence of the varied phosphonic acid modifications on the NiTi particles, which is in stark contrast to the unmodified sample's lack of these peaks. It is worth noting that these samples were prepared six months before analysis, suggesting that the phosphonic acid surface modifications remain stable over extended periods. An additional point worth highlighting is the observation of very faint silicon (Si) signals in the survey scans. The Si signals can be attributed to the areas of the poly-K coated glass coverslips where the nanoparticle coverage is thin, thus allowing detection of Si present in the glass. In the detailed peak fitting analysis of the high-resolution spectra, the $Ni2p_{3/2}$ peaks primarily exhibit a binding energy of 855.6 eV, indicative of the oxide form of nickel, with a smaller shoulder peak suggesting the presence of metallic nickel as well. The $Ti2p_{3/2}$ peak, observed at a binding energy of 458.5 eV, corroborates the predominance of titanium oxide in the composition of the nanoparticles. These findings are consistent

Table 2
Nickel, Titanium, and Phosphorus content analysis by ICP-OES of the nanoparticles before coating the coverslips.

Modification	Ni (%)	Ti (%)	P (%)
Unmodified NiTi	37.5	27.7	–
ODPA on NiTi	22.4	13.4	0.1
12-NH_2 on NiTi	1.2	0.7	0.7
COOHPA on NiTi	13.1	8.5	0.2
Ceftriaxone on NiTi	5.1	3.3	0.2
Vancomycin on NiTi	11.5	8.1	0.3

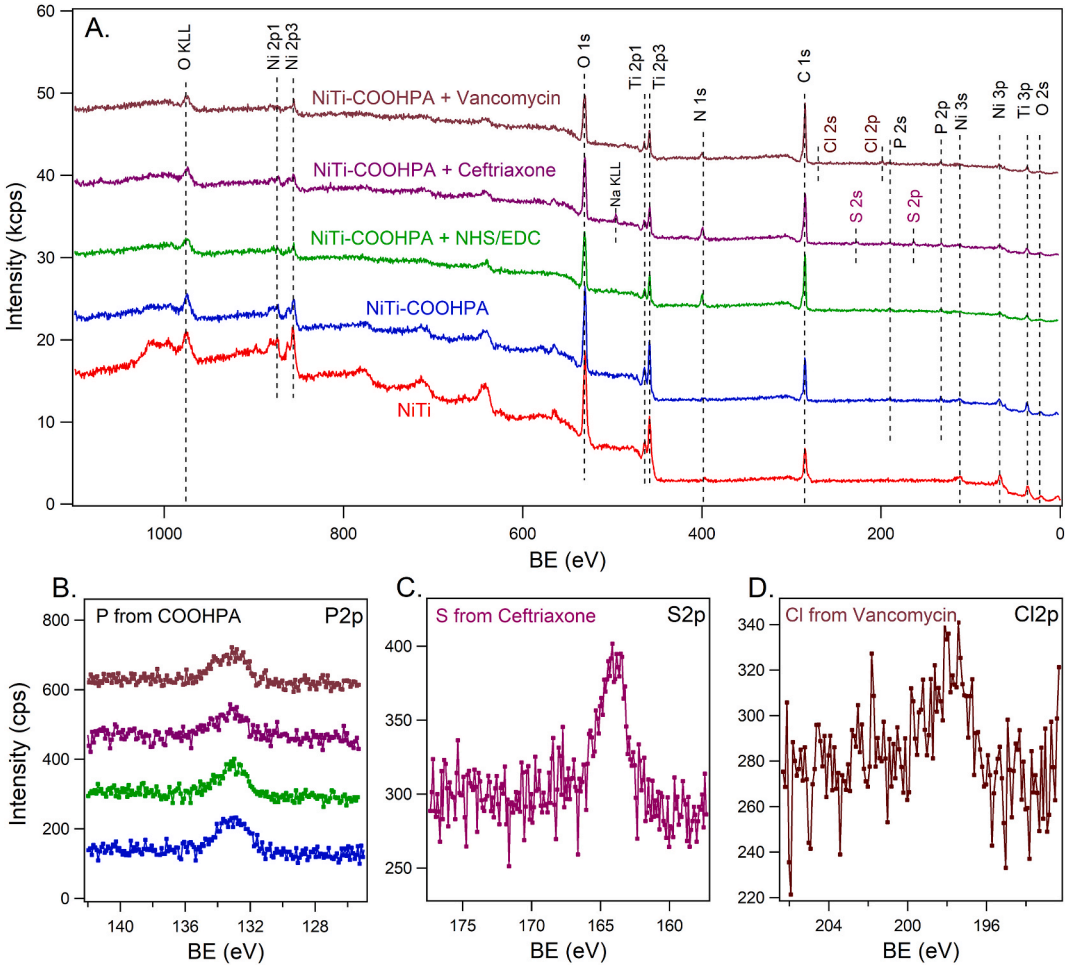

Fig. 5. XPS analysis of NiTi nanoparticles and their modifications. (A) Compositional survey scans of the original (red), COOHPA-modified (blue), NHS-ester (magenta), and antibiotic-added (purple for ceftriaxone and brown for vancomycin) NiTi nanoparticles. (B) High-resolution P2p spectra for COOHPA-modified samples showing phosphorus from COOHPA. (C) S2p spectra for samples with ceftriaxone, illustrating the antibiotic's attachment. (D) Cl2p spectra for vancomycin-modified samples, confirming the presence of the antibiotic.

Table 3
Atomic concentration ratios of NiTi nanoparticles and their modifications, as calculated from selected peaks in XPS measurements.

Atomic Ratio	Sample Name				
	NiTi	NiTi-COOHPA	NiTi-COOHPA + NHS/EDC	NiTi-COOHPA + Ceftriaxone	NiTi-COOHPA + Vancomycin
C (1s)	34.7%	38.3%	53.2%	48.9%	56.3%
O (1s)	42.7%	40.2%	28.8%	28.1%	27.1%
Ti (2p)	10.1%	9.7%	4.9%	5.1%	5.4%
Ni (2p3)	9.3%	7.4%	3.1%	4.7%	4.2%
N (1s)	3.2%	2.5%	8.1%	8.0%	4.2%
P (2p)	–	1.9%	1.9%	1.9%	1.8%
S (2p)	–	–	–	1.7%	–
Cl (2p)	–	–	–	–	1.0%
Na (1s)	–	–	–	1.6%	–

with the expected surface chemistry of NiTi nanoparticles undergoing oxidation in ambient conditions. Furthermore, the $P2p_{3/2}$ peak fitting analysis across all phosphonic acid-modified samples yields a binding energy of 133.0 eV, reinforcing the phosphorus signal identified in Fig. 5 and confirming the presence of phosphonic acid modifications.

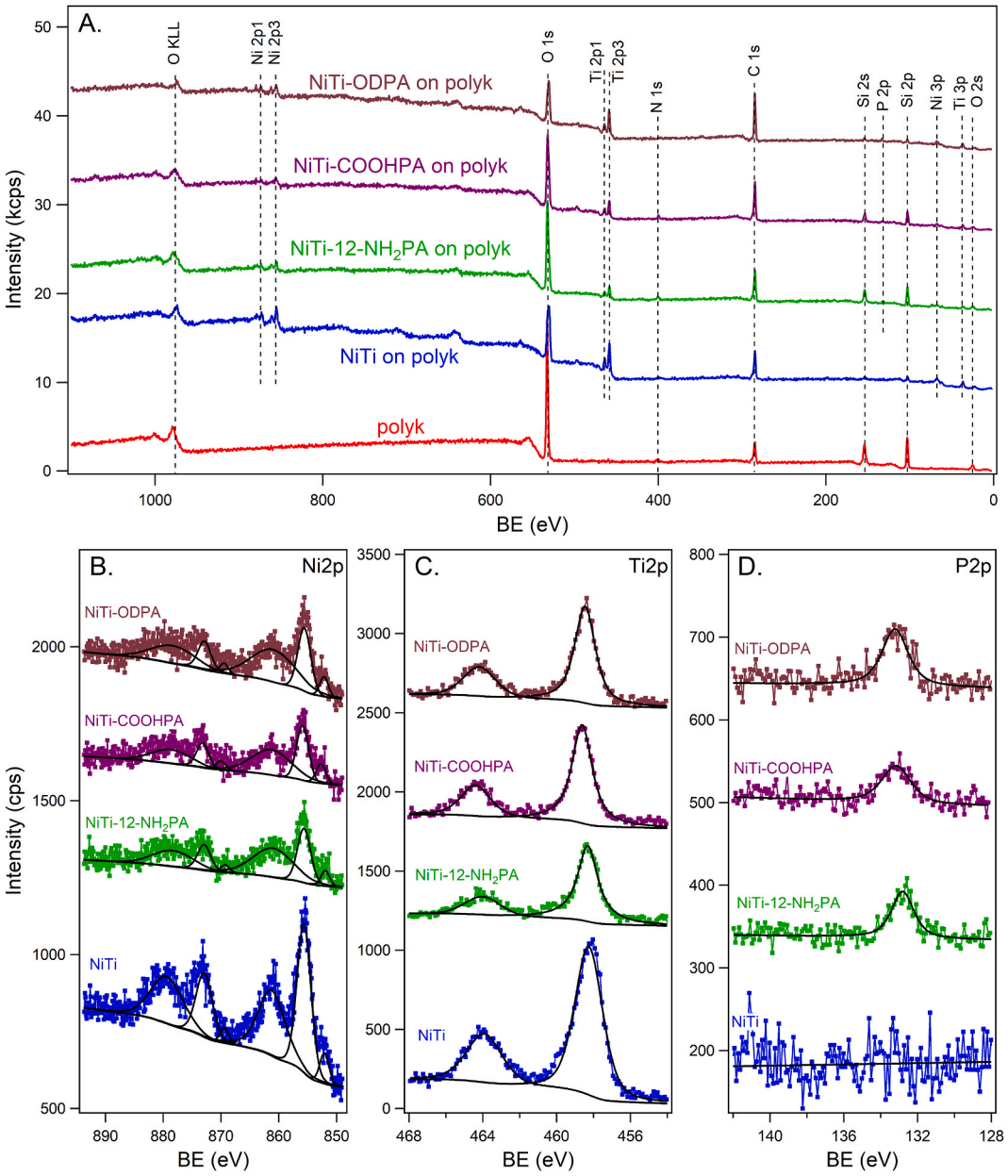

Fig. 6. XPS characterization of unmodified and phosphonic acid-modified NiTi nanoparticle coverage on poly-K coated coverslips. (A) Compositional survey scans of bare coverslip (red), unmodified NiTi-coated coverslip (blue), and coverslips coated with 12-NH_2PA (green), COOHPA (purple), or ODPA (brown)-modified NiTi nanoparticles. (B–D) High-resolution Ni2p, Ti2p, and P2p spectra.

3.5. Particle size and elemental analysis of NiTi on coverslips by SEM/EDS

SEM was used to confirm that the spherical-shaped NiTi nanoparticles were adhered to the poly-K-coated coverslips before and after cell culture. EDS mapping was used to identify the elemental composition of the unmodified and modified nanoparticles compared to the ICP-OES data. We previously performed a detailed SEM analysis to confirm that both unmodified and modified NiTi were composed of uniform spherical nanoparticles with typical particle diameters <100 nm [34]. As previously reported, there were no visible changes in the morphology of the nanoparticles after each modification when compared to the unmodified NiTi nanoparticles [34]. First, the presence and agglomeration of the nanoparticles on the coverslips were confirmed by capturing SEM images (Figs. 7 and 8). When plain poly-K-coated coverslips were analyzed by EDS, silicon, oxygen, potassium, sodium, aluminum, zinc, gold, palladium, titanium, and chlorine were detected. Gold and palladium from the thin layer of sputter coating were observed on the plain poly-K coated coverslips. This coating was applied to minimize the conductive surface of the glass and formed a thinner and more

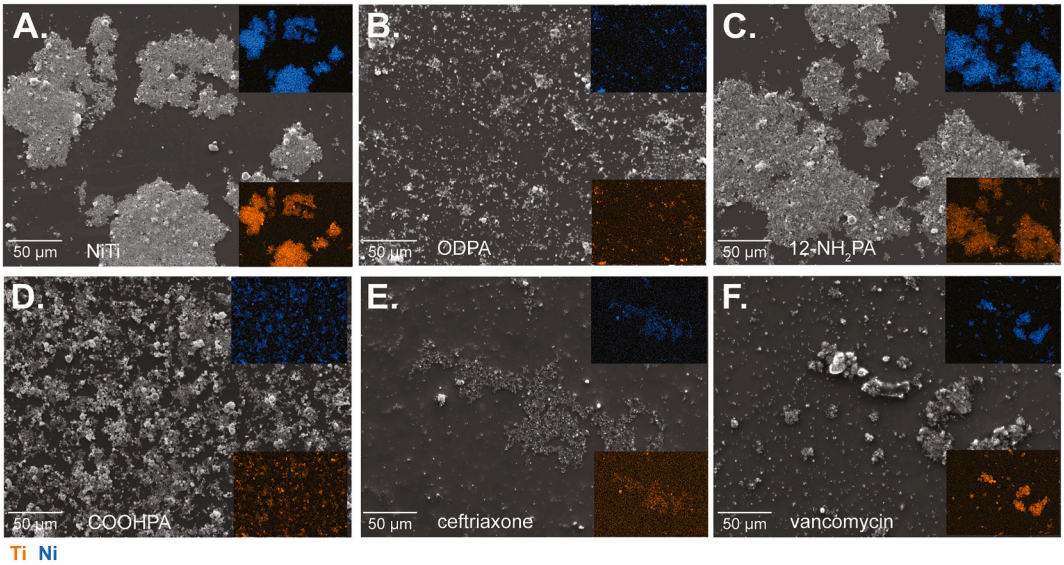

Fig. 7. SEM images at 600 × with corresponding EDS of a site representation of each poly-K-coated coverslips with nanoparticles before cell culture of (A) unmodified NiTi, (B) NiTi modified with ODPA, (C) NiTi modified with 12-NH_2PA (D) NiTi modified with COOHPA (E) NiTi modified with ceftriaxone, and (F) NiTi modified with vancomycin. Nickel (blue color mapping) and titanium (orange color mapping) with the microscope can be detected for each coverslip analyzed.

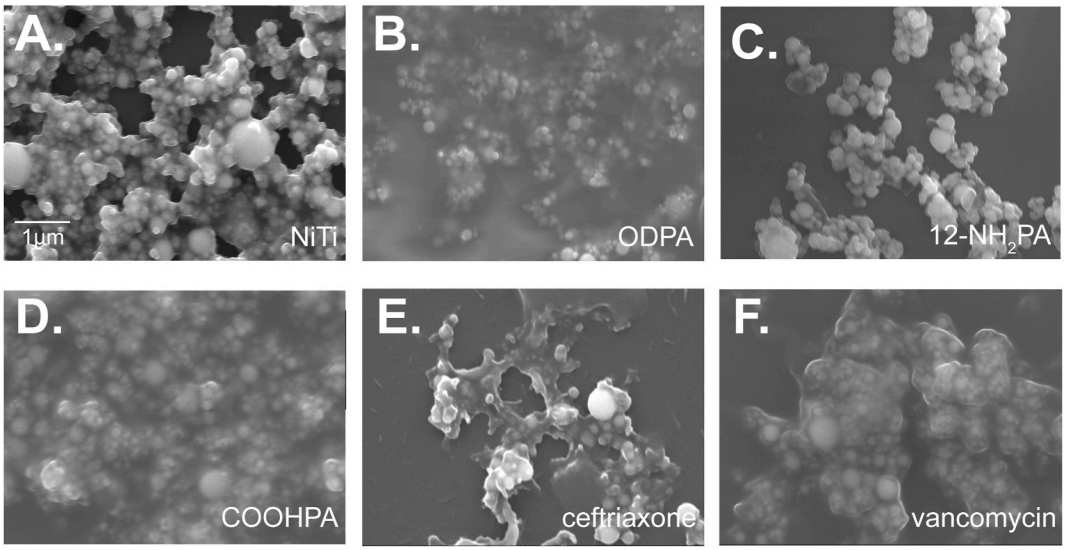

Fig. 8. SEM images at 20,000 × of each poly-K-coated coverslips with nanoparticles before cell culture of (A) unmodified NiTi, (B) NiTi modified with ODPA, (C) NiTi modified with 12-NH_2PA (D) NiTi modified with COOHPA (E) NiTi modified with ceftriaxone, and (F) NiTi modified with vancomycin.

uniform coating than carbon coating. A low amount of titanium was observed as a part of the glass content of the plain poly-K-coated coverslips, but no nickel content was detected. No particles were observed on the plain poly-K coated coverslips as expected. When the unmodified and modified nanoparticles adhered to the poly-K-coated coverslips, nickel and titanium elemental composition content were distributed throughout the surface of the coverslip before and after cell culture (Figs. 7 and 9). Furthermore, EDS mapping confirmed the presence of nickel and titanium distributed homogenously across the sample images. Phosphorus was also detected in all the modified NiTi nanoparticles when the nanoparticles were magnified more than 4000× (not shown) as expected due to the phosphonic acid head group [34].

The overall agglomeration of the particles observed in Figs. 7 and 8 is likely due to increased interaction between the surface charge of the particles [34]. It has also been demonstrated that the agglomerated particles are difficult to separate due to the densely packed alkyl chain films [34,68]. Several methods can be used to minimize agglomeration, including sonication, diluting the samples, or

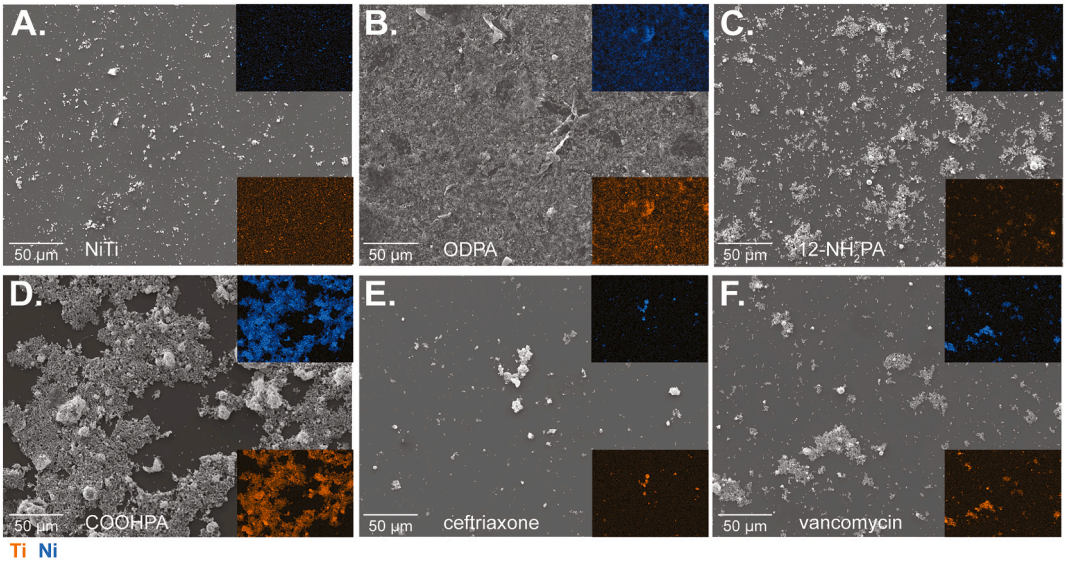

Fig. 9. SEM images at 600 × with corresponding EDS of a site representation of each poly-K-coated coverslips with nanoparticles after cell culture of (A) unmodified NiTi, (B) NiTi modified with ODPA, (C) NiTi modified with 12-NH_2PA (D) NiTi modified with COOHPA (E) NiTi modified with ceftriaxone, and (F) NiTi modified with vancomycin. Nickel (blue color mapping) and titanium (orange color mapping) with the microscope.

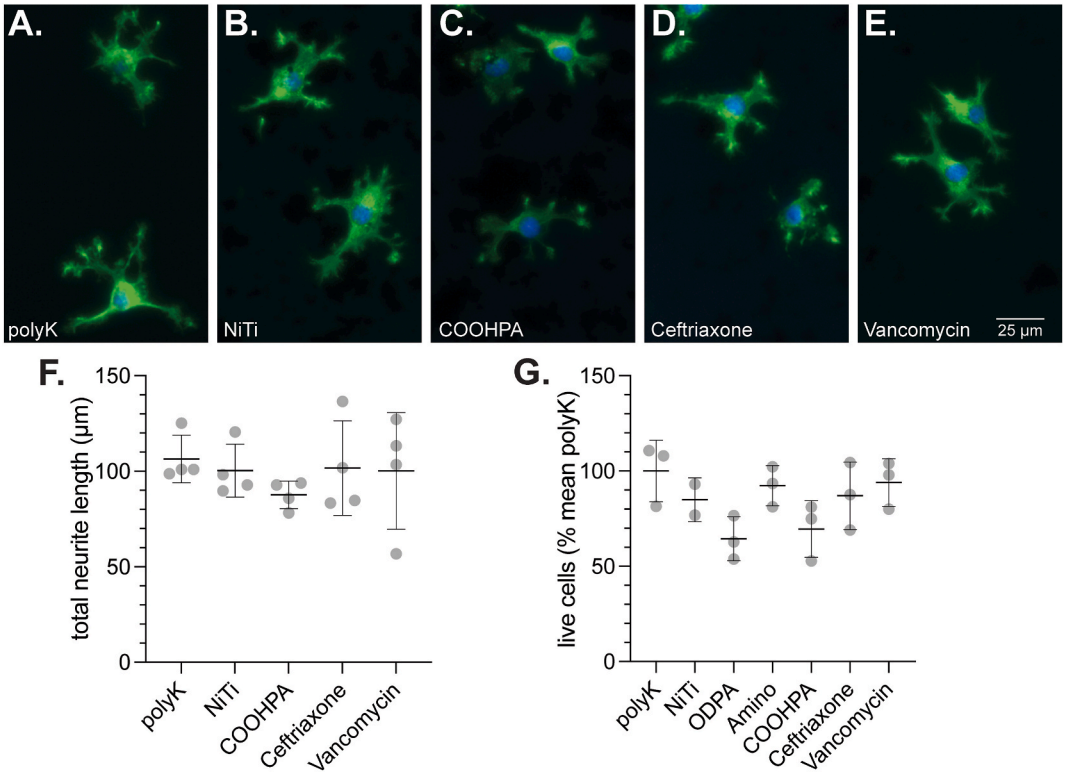

Fig. 10. NiTi substrates with various modifications do not alter the neurite extension properties of differentiating B35 cells. Cells labeled for F-actin (green) and nuclei (blue) were grown on coverslips coated with (A) poly-K only or (B) NiTi, (C) NiTi-COOHPA, (D) NiTi-COOHPA-ceftriaxone, (E) NiTi-COOHPA-vancomycin. (F) Mean total neurite length per cell measurements indicate no significant differences between cells grown on different surface coatings (G) A live/dead assay confirms that cell survival is comparable between cells grown on NiTi-coated surfaces and on poly-K alone. Mean + SD. $p > 0.05$. One-way ANOVA with Tukey's multiple comparisons.

adding surfactants, but the complete dissociation of agglomerates is unlikely [63,68,69]. 12-NH_2PA, COOHPA, and the antibiotic modifications are more hydrophilic than ODPA, which accounts for their more uniform distribution on the hydrophilic poly-K coated coverslips [70]. Conversely, EDS mapping indicates that the hydrophobic ODPA did not adhere to poly-K coated coverslips as readily as the other modifications (Fig. 7B); NiTi-ODPA agglomerates were likely washed away before analysis.

SEM images were also collected from coated coverslips after cell culture. All these coverslips were washed multiple times with phosphate buffer and incubated with cell culture medium and cells at physiological conditions. After cell culture, coverslips were washed with saline and water for SEM and EDS analysis. Especially for NiTi functionalized with antibiotics, individual nanoparticles coated the coverslips uniformly, generating a topography at subcellular scales for interaction with cells (Fig. 7). Modified NiTi nanoparticles and aggregates were regularly distributed on a similar scale as the somata of B35 cells, which have a diameter of ≈25 μm and neurite extensions of 10–40 μm (see Fig. 9). Cells plated on these surfaces can therefore be expected to interact extensively with the NiTi coating. The presence of nickel and titanium on the poly-K coated coverslips after cell culture (Fig. 9) confirms that the nanoparticle coatings withstand the numerous washes and extended time at physiological conditions associated with cell culture. The distortion of the spherical nanoparticles observed in samples analyzed after cell culture (Fig. 9) could be due to interactions with physiological saline and medium required for mammalian cell culture [51,71,72].

3.6. B35 cell differentiation on surfaces coated with NiTi

B35 cells differentiated on poly-K extended neurites with a total length of ≈100 μm (Fig. 10A). Comparable morphology was observed in cells grown on bare NiTi (Fig. 10B), NiTi modified with COOHPA (Fig. 10C), and NiTi-COOHPA functionalized with antibiotics ceftriaxone (Fig. 10D) and vancomycin (Fig. 10E) [73]. The mean total neurite length of B35 cells differentiated on NiTi solutions did not significantly differ from control cells on coverslips coated with only poly-K (Fig. 10F). Furthermore, a live/dead assay showed no difference in cell survival on coverslips coated with poly-K and NiTi solutions (Fig. 10G). These data indicate that NiTi-based coatings do not have adverse effects on cell survival or neurite extension and therefore have high potential as biocompatible surface coatings.

No statistical differences were detected in neurite extension or survival between cells grown on surfaces coated with only polyK or NiTi with or without modifications. However, the proportion of live cells on unmodified NiTi and NiTi modified only with ODPA and COOHPA was slightly reduced compared to cells on poly-K alone, NiTi-12-NH_2PA, and NiTi functionalized with antibiotics. This slightly reduced biocompatibility is not unexpected as unmodified NiTi and ODPA are non-polar and therefore less hospitable to cellular adhesion, which is promoted by surface wettability and charged functional groups [74]. COOHPA, although offering a negatively charged tail group, is still quite hydrophobic, and cells prefer to attach to cationic surfaces (eg. poly-K and 12-NH_2PA), as supported by our findings. The further addition of complex highly polar organic components (antibiotics) is also expected to support wettability and cellular adhesion. Similar effects were observed on modified graphene oxide films where primary hippocampal neurons grew well on all modified films, and positively charged modifications were slightly more effective in supporting the initiation of growth cones and neurite elongation than negatively charged modifications [75].

Cell culture analysis demonstrates that the morphology of cells on NiTi substrates is comparable to that of cells growing in standard physiological conditions (poly-K only) and that NiTi does not impair neurite extension or survival in B35 cells. The ability of all phosphonic-acid-modified NiTi to support neuronal adhesion, survival, and differentiation suggests that these structures have potential as a base for other modifications, such as growth factors [76] or extracellular matrix components [77]. For example, the extracellular matrix (ECM) proteins collagen and laminin are secreted very early in development [78] and provide critical binding and signaling functionality that promote cell adhesion, migration, and morphological development for many cell types [79]. Functionalizing potential NiTi coatings with modified phosphonic acid films that isolate and stabilize the NiTi core while providing a biomimetic interface with covalently bound ECM molecules could significantly promote the integration of reconstructive implants. Furthermore, surface-related properties, such as free energy (or wettability) and surface roughness are important parameters for cell-surface interactions and adhesion behavior [80]. Although it is necessary to minimize any damage to NiTi alloy's mechanical properties, especially shape memory, there are a number of ways that the NiTi surface could be improved by introducing surface modifications that promote wettability and using coating techniques to generate topographical surfaces that best mimic extracellular matrix structures.

3.7. Antimicrobial testing

Four strains of bacteria were chosen for testing with the functionalized NiTi, based on the mechanism of action of the antibiotics. Vancomycin, a glycopeptide inhibitor that prevents formation of the cell wall by binding to the peptidoglycan precursor, was examined with two Gram-positive bacterial strains [81,82]. Ceftriaxone is a third-generation β-lactam drug that prevents the synthesis of the cell wall by binding transpeptidases, resulting in loss of peptidoglycan cross-linking. It targets both Gram-positive and negative bacteria, preventing growth and inducing osmotic lysis [41]. Here we demonstrate that covalent anchoring of these antibiotics to the phosphonic acid film on NiTi does not interfere with their ability to bind at their active sites and exert their antimicrobial action.

We observed no inhibition of bacterial growth with poly-K, unmodified NiTi, or NiTi modified with COOHPA, 12-NH_2PA, or ODPA (data not shown), suggesting that NiTi and phosphonic acid films do not exert any inherent antimicrobial activity as has been reported to result from leached Ni from the coating [65].

S. epidermidis was not inhibited at a low dose (37.5 μg) of ceftriaxone but did display significant inhibition at higher doses (375 and 750 μg). *E coli* and *S. marcescens* displayed inhibition at all doses of ceftriaxone, but inhibition was significantly greater at 375 μg and

750 μg than at the low dose. *B. subtilis* demonstrated consistent inhibition by all doses of ceftriaxone. Inhibition of *B. subtilis* by NiTi functionalized with ceftriaxone was retained even after mammalian cell culture suggesting that the functionalized coating was stable through prolonged exposure to physiological conditions (Fig. 11A).

The Gram-negative strains, *E. coli* and S. *marcescens* (SM6) had variable responses to NiTi functionalized with vancomycin. Apart from inconsistent results at the low dose (37.5 μg), *S. marcescens* was not inhibited by the higher doses of vancomycin. Conversely, *E. coli* was significantly inhibited at higher antibiotic doses despite the inconsistent response at the lower dose. *S. epidermidis* did not respond to the lower dose but had an increasingly greater zone of inhibition as the antibiotic dose increased (Fig. 11B). This is expected as the reported effective dose of vancomycin against this strain of *S. epidermidis* is 2 mg/mL [83] and the concentration of vancomycin in our 0.75 mg/mL solution of vancomycin-functionalized NiTi is only 280 μg/ml. Again, NiTi functionalized with vancomycin maintained antimicrobial efficacy against *B. subtilis* consistently at all concentrations and after mammalian cell culture in physiological conditions.

A variable response in the inhibition of bacterial growth with vancomycin on the Gram-negative *E. coli* was expected due to the mechanism of the antibiotic targeting cell wall formation of Gram-positive bacteria. Previous studies have shown that the susceptibility of *E. coli* to vancomycin can change under varying growth conditions [84–86]. Interestingly, little difference in the degree of inhibition was found between 375 and 750 μg of antibiotic-functionalized NiTi in many cases, suggesting that the antibiotic linked to the nanoparticles had a limited range of diffusion as expected. Consistent with our findings, NiTi alone was previously found to be ineffective in generating anti-bacterial effects [87]. Some antibacterial efficacy was obtained by performing physical modifications such as heat, scoring the surface, or the addition of silver [88–90]. [91,92] By linking antibiotics to NiTi, instead of directly on titanium implant devices, we greatly expand the potential application of these passivated, functionalized nanoparticles for use as engineered coatings on diverse instruments and devices.

4. Conclusions

In this study, NiTi nanoparticles were modified with ordered phosphonic acids films containing various types of terminal groups, (methyl, amino, and carboxylic acid) and the carboxylic acid terminal group was further functionalized by coupling to two antibiotics: ceftriaxone and vancomycin. Then, unmodified, and modified NiTi were coated onto poly-K coated coverslips to determine their biocompatibility with cultured differentiating B35 neuroblastoma cells. Modified nanoparticles were characterized after synthesis, in solution, and as a coating on coverslips before and after cell culture. ATR- IR and XPS spectroscopy showed that the phosphonic acid modifications (1.9 % P atomic composition by XPS) were present on the NiTi surface and were stable for 18 months. ICP-OES data confirmed and quantified that the nanoparticles were present in the vials before the solution was prepared for coating the coverslips. SEM/EDS mapping studies were done after the modified or unmodified NiTi nanoparticles were coated on the coverslips before and after cell culture and showed that the nanoparticles were evenly distributed, with variations occurring at a smaller scale than the size of cell somata and neurite extensions. Furthermore, the modifications were intact in nanoparticle coatings on the coverslips after mammalian cell culture in physiological conditions. Quantitative analysis of differentiating B35 cell morphology indicated that cells with a total neurite length averaged 100 μm on poly-K and on modified or unmodified NiTi. Furthermore, NiTi coatings had no negative effects on cell survival. Inhibition of *Escherichia coli* and *Serratia marcescens* (SM6) by NiTi nanoparticles functionalized with ceftriaxone was achieved at doses of 375 and 750 μg, respectively. *Bacillus subtilis* growth was inhibited by only 37.5 μg. Additionally, *B. subtilis* was inhibited at all doses by NiTi-vancomycin even after culture with mammalian cells. Phosphonic acid-modified NiTi nanoparticles are promising candidates as coatings on osteopathic or nerve implants to promote cellular adhesion and growth. In addition to reducing the amount of repeat hard tissue surgery replacements required, these coatings may also increase the lifetime of osteopathic implants. The phosphonic acid modifications also provide substrates amenable to additional chemical functionalization that may further enhance biocompatibility. Surgical tools and equipment, wound dressings, and other medical devices could benefit from these surface modifications.

Data availability statement

All data to support the conclusions have been either provided or are otherwise publicly available.

CRediT authorship contribution statement

Sarah McGlumphy: Writing – review & editing, Writing – original draft, Methodology, Investigation. **Aakriti Damai:** Writing – review & editing, Writing – original draft, Methodology, Investigation. **Lena Salameh:** Writing – review & editing, Investigation, Data curation. **Gabriell B. Corbin:** Writing – review & editing, Investigation. **Qiang Wang:** Writing – original draft, Investigation, Formal analysis. **John Markiewicz:** Writing – review & editing, Writing – original draft, Visualization, Methodology, Investigation. **Jennifer J. Mosher:** Writing – review & editing, Writing – original draft, Visualization, Validation, Supervision, Methodology, Investigation, Formal analysis, Data curation, Conceptualization. **Nadja Spitzer:** Writing – review & editing, Writing – original draft, Visualization, Supervision, Resources, Methodology, Formal analysis, Data curation. **Rosalynn Quiñones:** Writing – review & editing, Writing – original draft, Visualization, Validation, Supervision, Resources, Methodology, Investigation, Funding acquisition, Formal analysis, Data curation, Conceptualization.

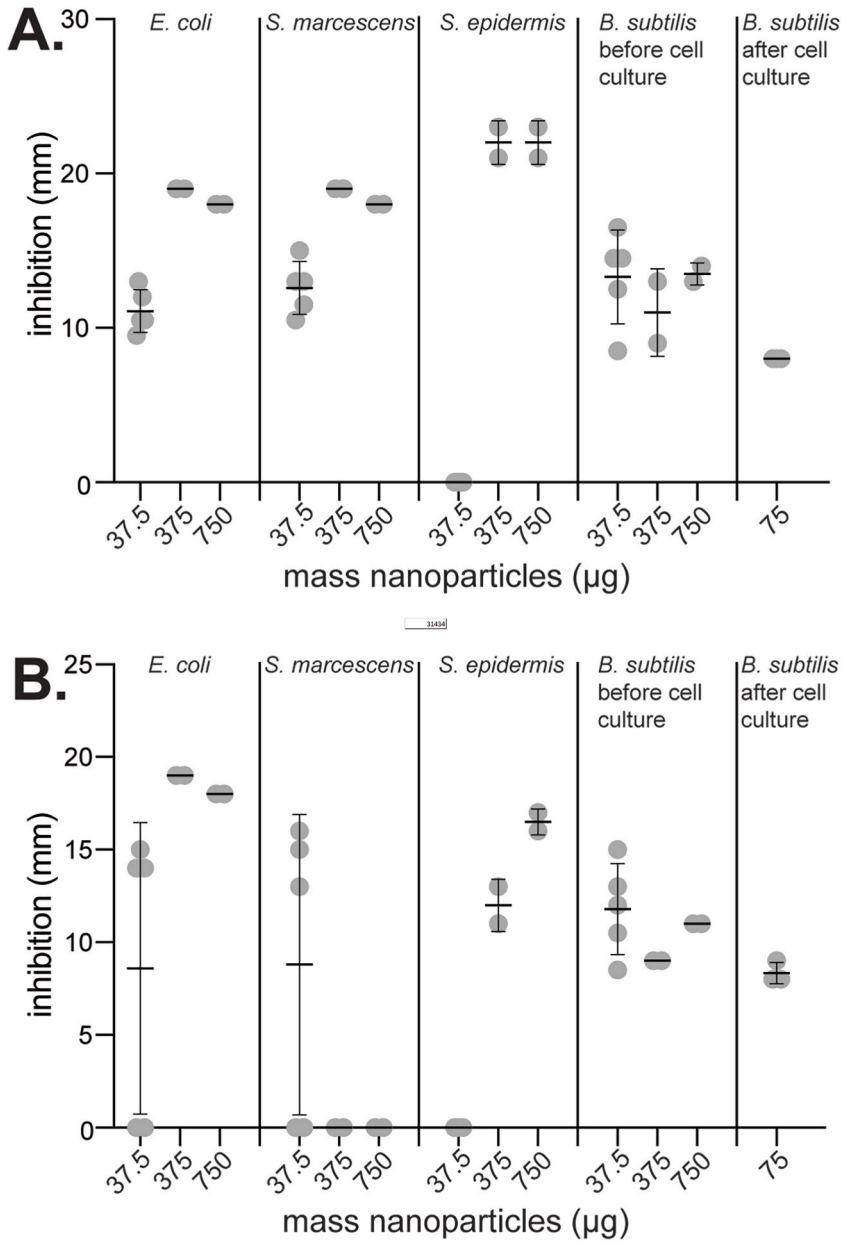

Fig. 11. Inhibition (mm diameter) of the tested bacterial strains by NiTi functionalized with (A) ceftriaxone or (B) vancomycin for doses of 37.5, 375 and 750 µg. NiTi functionalized with either antibiotic (75 µg) and collected from coverslips after mammalian cell culture also effectively inhibited the growth of *B. subtilis*.

Declaration of competing interest

The authors declare the following financial interests/personal relationships which may be considered as potential competing interests: Rosalynn Quinones reports financial support was provided by National Science Foundation. Rosalynn Quinones reports financial support was provided by NASA West Virginia Space Grant Consortium. Rosalynn Quinones reports financial support was provided by West Virginia Higher Education Policy Commission.

Acknowledgements

This work was funded by a National Science Foundation (NSF) (Award # CHE1828358), NASA West Virginia Space Grant Consortium (Training Grant # NNX15AI01H and 80NSSC20M0055), West Virginia Higher Education Policy Commission under the grant

numbers HEPC.dsr.18.7. And dsr.20.16 amend. 1.1, and Research Challenge Grant (RCG23-009). *S. marcescens* strain SM6 and *S. epidermidis* cultures were graciously donated by Dr. Lydia Bobomolnaya and Dr. Hongwei Wu, respectively. We would like to thank Samantha Garretson, Deben Shoup, Hannah Smith, and Trenton Reed for collecting preliminary data for this project.

Abbreviations

NiTi	nitinol
SAMs	self-assembled monolayers
ODPA	octadecylphosphonic acid
COOHPA	16-phosphonohexadecanoic acid
12-NH_2PA	12-aminododecylphosphonic acid
NCAMS	neural cell adhesion molecules
DLS	dynamic light scattering
ATR-IR	attenuated total reflectance infrared spectroscopy
ICP-OES	inductively coupled plasma optical emission spectroscopy
SEM	scanning electron microscopy
EDS	energy dispersive X-ray spectroscopy
XPS	X-ray photoelectron spectroscopy
poly-K	poly-L-lysine
MIC	minimum inhibitory concentration
DAPI, 4′	6-diamidino-2-phenylindole
THF	tetrahydrofuran
DMEM	Dulbecco's Modified Eagle Medium
FBS	fetal bovine serum
Pen/Strep	Penicillin Streptomycin
PFA	paraformaldehyde
BSA	bovine serum albumin
PBS	phosphate-buffered saline
SM6	serratia marcescens

References

[1] N.K.E. Awad, Y.S. S.L.Morsy, *A Review of TiO_2 NTs on Ti metal: Electrochemical synthesis, Functionalization and potential Use as bone implants*, Mater. Sci. Eng., C 76 (2017) 1401–1412, https://doi.org/10.1016/j.msec.2017.02.150.
[2] L. Patnaik, S. Ranjan Maity, S. Kumar, Status of nickel free stainless steel in biomedical field: a review of last 10 years and what else can be done, Mater Today Proc 26 (2020) 638–643, https://doi.org/10.1016/j.matpr.2019.12.205.
[3] N. Eliaz, Corrosion of metallic biomaterials: a review, Materials 12 (3) (2019), https://doi.org/10.3390/ma12030407.
[4] K. Prasad, et al., Metallic biomaterials: current challenges and Opportunities, Materials 10 (8) (2017), https://doi.org/10.3390/ma10080884.
[5] J.N.C. Liao, G. Tan, G. Ni, H. Pan, Conducting Polypyrrole nanotube Arrays as an implant surface: Fabricated on biomedical titanium with FineTunability by means of Template-free Electrochemical Polymerization, ChemPlusChem 79 (4) (2014) 530–534, https://doi.org/10.1002/cplu.201300385.
[6] M. Wang, et al., Understanding the passivation behavior and film chemistry of four corrosion-resistant alloys in the simulated flue gas condensates, Mater. Today Commun. 31 (2022) 103567, https://doi.org/10.1016/j.mtcomm.2022.103567.
[7] K.M. Kruszewski, et al., Reducing Staphylococcus aureus biofilm formation on stainless steel 316L using functionalized self-assembled monolayers, Mater Sci Eng C 33 (4) (2013) 2059–2069, https://doi.org/10.1016/j.msec.2013.01.023.
[8] A. Raman, et al., Understanding organic film behavior on alloy and metal oxides, Langmuir 26 (3) (2010) 1747–1754, https://doi.org/10.1021/la904120s.
[9] C.S. Barros, S.J. Franco, U. Müller, Extracellular matrix: functions in the nervous system, Cold Spring Harbor Perspect. Biol. 3 (1) (2011) a005108, https://doi.org/10.1101/cshperspect.a005108.
[10] Y.W. Fan, et al., Culture of neural cells on silicon wafers with nano-scale surface topograph, J. Neurosci. Methods 120 (1) (2002) 17–23, https://doi.org/10.1016/S0165-0270(02)00181-4.
[11] T. Limongi, et al., Nanostructured Superhydrophobic substrates Trigger the development of 3D neuronal Networks, Small 9 (3) (2013) 402–412, https://doi.org/10.1002/smll.201201377.
[12] N. Morgan, J. W.A.DiCello, R. Graham, Carbon and oxygen levels in nitinol alloys and the implications for medical device manufacture and durability, in: SMST, 2008.
[13] S.N.A. Strauß, S. Barcikowski, D. Kracht, J.W. Kuhbier, C. Radtke, K. Reimers, P.M. Voght, Adhesion, Vitality and Osteogenic differentiation Capacity of Adipose derived stem cells Seeded on nitinol nanoparticle coatings, PLoS One 8 (1) (2013) 1–11, https://doi.org/10.1371/journal.pone.0053309.
[14] N. Sharma, K. Gupta, Wire Spark Erosion Machining of Ni rich NiTi shape memory alloy for Bio-medical applications, Procedia Manuf. 35 (2019) 401–406, https://doi.org/10.1016/j.promfg.2019.05.059.
[15] C. Watson, et al., Performance of a hydrogel coated nitinol with Oligonucleotide-modified nanoparticles within Turbulent conditions of blood-Contacting devices, Cardiovasc Eng Technol 14 (2) (2023) 239–251, https://doi.org/10.1007/s13239-022-00650-2.
[16] A.K. Srivastava, et al., Examining the role of nickel and NiTi nanoparticles promoting inflammation and angiogenesis, J. Immunopharm. 19 (1) (2022) 61–73, https://doi.org/10.1080/1547691X.2022.2080307.
[17] C. Zhao, et al., Graphene oxide based coatings on nitinol for biomedical implant applications: effectively promote mammalian cell growth but kill bacteria, RSC Adv. 6 (44) (2016) 38124–38134, https://doi.org/10.1039/C6RA06026A.
[18] B. Clarke, et al., Influence of nitinol wire surface treatment on oxide thickness and composition and its subsequent effect on corrosion resistance and nickel release, J. Biomed. Mater. Res. 79A (2006) 61–70, https://doi.org/10.1002/jbm.a.30720.
[19] N. Shevchenko, M.T. Pham, M.F. Maitz, Studies of surface modified NiTi alloy, Appl. Surf. Sci. 235 (1–2) (2004) 126–131, https://doi.org/10.1016/j.apsusc.2004.05.273.

[20] H.H. Huang, Surface characterizations and corrosion resistance of nickel-titanium orthodontic archwires in artificial saliva of various degrees of acidity, J. Biomed. Mater. Res. 74A (4) (2005) 629–639, https://doi.org/10.1002/jbm.a.30340.
[21] N. Pandis, C.P. Bourauel, Nickel-titanium (NiTi) Arch wires: the Clinical significance of super Elasticity, Semin. Orthod. 16 (4) (2010) 249–257, https://doi.org/10.1053/j.sodo.2010.06.003.
[22] G.B. Kauffman, I. Mayo, The story of nitinol: the Serendipitous Discovery of the memory metal and its applications, Chem. Educ. 2 (2) (1997) 1–21, https://doi.org/10.1007/s00897970111a.
[23] M.S. Safavi, et al., Surface modified NiTi smart biomaterials: surface engineering and biological compatibility, Current Opinion in Biomedical Engineering 25 (2023) 100429, https://doi.org/10.1016/j.cobme.2022.100429.
[24] S.A. Shabalovskaya, Physicochemical and biological aspects of Nitinol as a biomaterial, Int. Mater. Rev. 46 (5) (2001) 233–250, https://doi.org/10.1179/095066001771048745.
[25] N.G. Donghui Wang, Jinhua Li, Yuqin Qiao, Hongqin Zhu, Xuanyong Liu, Selective Tumor cell inhibition effect of Ni−Ti layered Double Hydroxides thin films Driven by the Reversed pH Gradients of Tumor cells, ACS Appl. Mater. Interfaces 7 (2015) 7043–7054, https://doi.org/10.1021/acsami.5b01087.
[26] A. Maho, et al., Electrochemical Investigation of nitinol/Tantalum hybrid surfaces modified by Alkylphosphonic self-assembled monolayers, Electrochim. Acta 116 (2014) 78–88, https://doi.org/10.1016/j.electacta.2013.11.008.
[27] S. Devillers, et al., Induction heating Vs Conventional heating for the Hydrothermal treatment of nitinol and its subsequent 2-(Methacryloyloxy)ethyl 2-(trimethylammonio)ethyl phosphate coating by surface-Initiated Atom transfer Radical Polymerization, ACS Appl. Mater. Interfaces 3 (10) (2011) 4059–4066, https://doi.org/10.1021/am200912k.
[28] Ž. Petrović, et al., Modification of a nitinol surface by phosphonate self-assembled monolayers, J. Electrochem. Soc. 158 (10) (2011) F159–F165, https://doi.org/10.1149/1.3617651.
[29] M. Liu, et al., Stabilized Hemocompatible coating of nitinol devices based on Photo-Cross-linked Alginate/Heparin Multilayer, Langmuir 23 (18) (2007) 9378–9385, https://doi.org/10.1021/la7002996.
[30] T.B. McPherson, H.S. Shim, K. Park, Grafting of PEO to glass, nitinol, and pyrolytic carbon surfaces by gamma irradiation, J. Biomed. Mater. Res. 38 (4) (1997) 289–302, https://doi.org/10.1002/(SICI)1097-4636(199724)38:4%3C289::AID-JBM1%3E3.0.CO;2-K.
[31] U.R. Dahiya, et al., Modified surface composition and biocompatibility of core-Shell nitinol nanoparticles Fabricated via Laser Ablation of differently Passivized targets, Frontiers in Materials 9 (2022), https://doi.org/10.3389/fmats.2022.855705.
[32] M. Yao, et al., Metallic nanoparticle-Doped oxide Semiconductor film for bone Tumor Suppression and bone regeneration, ACS Appl. Mater. Interfaces 14 (42) (2022) 47369–47384, https://doi.org/10.1021/acsami.2c10672.
[33] J. Ryhänen, et al., Biocompatibility of nickel-titanium shape memory metal and its corrosion behavior in human cell cultures, J. Biomed. Mater. Res. 35 (4) (1997) 451–457, https://doi.org/10.1002/(SICI)1097-4636(19970615)35:4%3C451::AID-JBM5%3E3.0.CO;2-G.
[34] R. Quiñones, et al., Fabrication of phosphonic acid films on nitinol nanoparticles by dynamic covalent assembly, Thin Solid Films 642 (C) (2017) 195–206, https://doi.org/10.1016/j.tsf.2017.09.048.
[35] R. Quiñones, E.S. Gawalt, Polystyrene Formation on monolayer-modified nitinol effectively controls corrosion, Langmuir 24 (19) (2008) 10858–10864, https://doi.org/10.1021/la801906e.
[36] I. Milošev, M. Metikoš-Huković, Ž. Petrović, Influence of preparation methods on the properties of self-assembled films of octadecylphosphonate on Nitinol: XPS and EIS studies, Mater. Sci. Eng. C 32 (8) (2012) 2604–2616, https://doi.org/10.1016/j.msec.2012.08.010.
[37] R. Quiñones, E.S. Gawalt, Study of the formation of self-assembled monolayers on nitinol, Langmuir 23 (20) (2007) 10123–10130, https://doi.org/10.1021/la701110p.
[38] A. Hasan, V. Saxena, L.M. Pandey, Surface functionalization of Ti6Al4V via self-assembled monolayers for improved protein Adsorption and fibroblast adhesion, Langmuir 34 (11) (2018) 3494–3506, https://doi.org/10.1021/acs.langmuir.7b03152.
[39] M. Monaco, et al., Worldwide Epidemiology and antibiotic resistance of Staphylococcus aureus, Curr. Top. Microbiol. Immunol. 409 (2017) 21–56, https://doi.org/10.1007/82_2016_3.
[40] R.N. Palchesko, et al., Co-immobilization of active antibiotics and cell adhesion peptides on calcium based biomaterials, Mater Sci Eng C 40 (2014) 398–406, https://doi.org/10.1016/j.msec.2014.04.017.
[41] M.S. Haugan, A. Løbner-Olesen, N. Frimodt-Møller, Comparative activity of ceftriaxone, ciprofloxacin, and Gentamicin as a function of bacterial growth rate probed by Escherichia coli Chromosome Replication in the mouse Peritonitis model, Antimicrob. Agents Chemother. 63 (2) (2019) e02133, https://doi.org/10.1128/aac.02133-18, 18.
[42] M.S. de Oliveira, et al., Polymeric nanoparticle associated with ceftriaxone and Extract of Schinopsis Brasiliensis Engler against Multiresistant Enterobacteria, Pharmaceutics 12 (8) (2020) 695, https://doi.org/10.3390/pharmaceutics12080695.
[43] A.R. Hossein abadi, et al., Ceftriaxone sodium loaded onto polymer-lipid hybrid nanoparticles enhances antibacterial effect on gram-negative and gram-positive bacteria: effects of lipid - polymer ratio on particles size, characteristics, in vitro drug release and antibacterial drug efficacy, J. Drug Deliv. Sci. Technol. 63 (2021) 102457, https://doi.org/10.1016/j.jddst.2021.102457.
[44] S.J. Metallo, et al., Using bifunctional polymers presenting vancomycin and fluorescein groups to direct anti-fluorescein antibodies to self-assembled monolayers presenting D-alanine-D-alanine groups, JACS 125 (15) (2003) 4534–4540, https://doi.org/10.1021/ja030045a.
[45] M. Assali, et al., Single-walled carbon nanotubes-ciprofloxacin nanoantibiotic: strategy to improve ciprofloxacin antibacterial activity, Int. J. Nanomed. 12 (2017) 6647–6659, https://doi.org/10.2147/IJN.S140625.
[46] N. Khatoon, et al., Ampicillin silver Nanoformulations against multidrug resistant bacteria, Sci. Rep. 9 (1) (2019) 6848, https://doi.org/10.1038/s41598-019-43309-0.
[47] J.E. Baio, D.J. Graham, D.G. Castner, Surface analysis tools for characterizing biological materials, Chem. Soc. Rev. 49 (11) (2020) 3278–3296, https://doi.org/10.1039/D0CS00181C.
[48] L. Portilla, M. Halik, Smoothly Tunable surface properties of aluminum oxide core–Shell nanoparticles by A Mixed-Ligand Approach, ACS Appl. Mater. Interfaces 6 (8) (2014) 5977–5982, https://doi.org/10.1021/am501155r.
[49] L. Patrone, et al., Versatility of aqueous micellar solutions for self-assembled monolayers engineering, Langmuir 20 (26) (2004) 11577–11582, https://doi.org/10.1021/la048133b.
[50] C.A.B.M. Otey, P. Maness, B35 neuroblastoma cells: an Easily Transfected, cultured cell model of central nervous system neurons, Methods and Applications for the Cell Biologist (2003) 287–300.
[51] R.J. Cooper, N. Spitzer, Silver nanoparticles at sublethal concentrations disrupt cytoskeleton and neurite dynamics in cultured adult neural stem cells, Neurotoxicology 48 (2015) 231–238, https://doi.org/10.1016/j.neuro.2015.04.008.
[52] L.R. Williams, et al., Spatial-Temporal progress of peripheral nerve regeneration within a silicone chamber: parameters for a bioassay, J. Comp. Neurol. 218 (4) (1983) 460–470, https://doi.org/10.1002/cne.902180409.
[53] N.J. Gardiner, Integrins and the extracellular matrix: Key mediators of development and regeneration of the sensory nervous system, Dev Neurobiol 71 (11) (2011) 1054–1072, https://doi.org/10.1002/dneu.20950.
[54] J.P. Myers, M. Santiago-Medina, T.M. Gomez, Regulation of axonal outgrowth and pathfinding by integrin-ECM interactions, Dev Neurobiol 71 (11) (2011) 901–923, https://doi.org/10.1002/dneu.20931.
[55] E. Meijering, et al., Design and validation of a tool for neurite tracing and analysis in fluorescence microscopy images, Cytometry 58A (2) (2004) 167–176, https://doi.org/10.1002/cyto.a.20022.
[56] K.S. MacLea, A.M. Trachtenberg, Complete Genome sequence of Staphylococcus epidermidis ATCC 12228 Chromosome and Plasmids, generated by long-Read Sequencing, Genome Announc. 5 (36) (2017), https://doi.org/10.1128/genomeA.00954-17.

[57] D.B. Adimpong, et al., Antimicrobial susceptibility of Bacillus strains isolated from primary Starters for African Traditional Bread Production and characterization of the Bacitracin Operon and Bacitracin Biosynthesis, Appl. Environ. Microbiol. 78 (22) (2012) 7903–7914, https://doi.org/10.1128/AEM.00730-12.

[58] I.V. Khilyas, et al., Genome sequence of Pigmented Siderophore-Producing strain Serratia marcescens SM6, Microbiol Resour Announc 8 (18) (2019), https://doi.org/10.1128/mra.00247-19, 10.1128/mra.00247-19.

[59] Y. Huang, et al., Determining the optimal ceftriaxone MIC for Triggering extended-spectrum β-Lactamase Confirmatory testing, J. Clin. Microbiol. 52 (6) (2014) 2228–2230, https://doi.org/10.1128/jcm.00716-14.

[60] C.-L. Lu, et al., Antimicrobial Susceptibilities of commonly Encountered bacterial isolates to Fosfomycin determined by agar dilution and disk diffusion methods, Antimicrob. Agents Chemother. 55 (9) (2011) 4295–4301, https://doi.org/10.1128/aac.00349-11.

[61] A.L. Barry, et al., Methods of measuring zones of inhibition with the Bauer-Kirby disk susceptibility test, J. Clin. Microbiol. 10 (6) (1979) 885–889, https://doi.org/10.1128/jcm.10.6.885-889.1979.

[62] K.R. Fiebelkorn, et al., Practical disk diffusion Method for Detection of inducible Clindamycin Resistance in Staphylococcus aureus and coagulase-negative Staphylococci, J. Clin. Microbiol. 41 (10) (2003) 4740–4744, https://doi.org/10.1128/jcm.41.10.4740-4744.2003.

[63] C. Minelli, et al., Sticky measurement problem: number concentration of agglomerated nanoparticles, Langmuir 35 (14) (2019) 4927–4935, https://doi.org/10.1021/acs.langmuir.8b04209.

[64] J. Austin, et al., Nanoparticle number concentration measurements by multi-angle dynamic light scattering, J Nanopart Res 22 (5) (2020) 108, https://doi.org/10.1007/s11051-020-04840-8.

[65] N. Ohtsu, S. Suginishi, M. Hirano, Antibacterial effect of nickel-titanium alloy owing to nickel ion release, Appl. Surf. Sci. 405 (2017) 215–219, https://doi.org/10.1016/j.apsusc.2017.02.037.

[66] C. Zhang, et al., Electrostatic interaction and surface S vacancies synergistically enhanced the photocatalytic degradation of ceftriaxone sodium, Chemosphere 311 (2023) 137053, https://doi.org/10.1016/j.chemosphere.2022.137053.

[67] A.T. Abafogi, et al., Vancomycin-conjugated polydopamine-coated magnetic nanoparticles for molecular diagnostics of Gram-positive bacteria in whole blood, J. Nanobiotechnol. 20 (1) (2022) 400, https://doi.org/10.1186/s12951-022-01606-3.

[68] B. Feichtenschlager, et al., Nanoparticle Assemblies as probes for self-assembled monolayer characterization: Correlation between surface functionalization and agglomeration behavior, Langmuir 28 (1) (2012) 741–750, https://doi.org/10.1021/la2023067.

[69] H. Sis, M. Birinci, Effect of nonionic and ionic surfactants on zeta potential and dispersion properties of carbon black powders, Colloids Surf. A Physicochem. Eng. Asp. 341 (1) (2009) 60–67, https://doi.org/10.1016/j.colsurfa.2009.03.039.

[70] E.S. Cole, et al., Chapter 8 - Confocal fluorescence microscopy for Tetrahymena thermophila, in: B. Matsumoto (Ed.), Methods in Cell Biology, Academic Press, 2002, pp. 337–359.

[71] A.B. Parsons-White, N. Spitzer, Environmentally relevant manganese overexposure alters neural cell morphology and differentiation in vitro, Toxicol. Vitro 50 (2018) 22–28, https://doi.org/10.1016/j.tiv.2018.02.015.

[72] S. Nadja, et al., Multipotent progenitor cells derived from adult peripheral blood of swine have high neurogenic potential in vitro, J. Cell. Physiol. 226 (12) (2011) 3156–3168, https://doi.org/10.1002/jcp.22670.

[73] I. Rishal, et al., WIS-neuromath enables versatile high throughput analyses of neuronal processes, Dev Neurobiol 73 (3) (2013) 247–256, https://doi.org/10.1002/dneu.22061.

[74] K. Webb, V. Hlady, P.A. Tresco, Relative importance of surface wettability and charged functional groups on NIH 3T3 fibroblast attachment, spreading, and cytoskeletal organization, J. Biomed. Mater. Res. 41 (3) (1998) 422–430, https://doi.org/10.1002/(SICI)1097-4636(19980905)41:3%3C422::AID-JBM12%3E3.0.CO;2-K.

[75] Q. Tu, et al., Effects of surface charges of graphene oxide on neuronal outgrowth and branching, Analyst 139 (1) (2014) 105–115, https://doi.org/10.1039/C3AN01796F.

[76] H. Li, et al., In vivo assessment of guided neural stem cell differentiation in growth factor immobilized chitosan-based hydrogel scaffolds, Biomaterials 35 (33) (2014) 9049–9057, https://doi.org/10.1016/j.biomaterials.2014.07.038.

[77] Š. Kubinová, et al., The use of superporous Ac-CGGASIKVAVS-OH-modified PHEMA scaffolds to promote cell adhesion and the differentiation of human fetal neural precursors, Biomaterials 31 (23) (2010) 5966–5975, https://doi.org/10.1016/j.biomaterials.2010.04.040.

[78] I. Leivo, et al., Appearance and distribution of collagens and laminin in the early mouse embryo, Dev. Biol. 76 (1) (1980) 100–114, https://doi.org/10.1016/0012-1606(80)90365-6.

[79] J.K. Kular, S. Basu, R.I. Sharma, The extracellular matrix: structure, composition, age-related differences, tools for analysis and applications for tissue engineering, J. Tissue Eng. 5 (2014) 2041731414557112, https://doi.org/10.1177/2041731414557112.

[80] V.C. Dinca, et al., Nickel–titanium alloy: Cytotoxicity evaluation on microorganism culture, Appl. Surf. Sci. 252 (2006) 4619–4624, https://doi.org/10.1016/j.apsusc.2005.07.093.

[81] S. Gardete, A. Tomasz, Mechanisms of vancomycin resistance in Staphylococcus aureus, J. Clin. Invest. 124 (7) (2014) 2836–2840, https://doi.org/10.1172/JCI68834.

[82] I.G. Boneca, G. Chiosis, Vancomycin resistance: occurrence, mechanisms and strategies to combat it, Expert Opin. Ther. Targets 7 (3) (2003) 311–328, https://doi.org/10.1517/14728222.7.3.311.

[83] D.C. Coraça-Huber, et al., Iron chelation destabilizes bacterial biofilms and potentiates the antimicrobial activity of antibiotics against coagulase-negative Staphylococci, Pathog Dis 76 (5) (2018), https://doi.org/10.1093/femspd/fty052.

[84] L.F. Neville, et al., In vivo targeting of Escherichia coli with vancomycin-Arginine, Antimicrob. Agents Chemother. 65 (4) (2021) e02416–e02420, https://doi.org/10.1128/aac.02416-20.

[85] Jonathan M. Stokes, et al., Cold stress makes Escherichia coli susceptible to glycopeptide antibiotics by altering outer Membrane Integrity, Cell Chem. Biol. 23 (2) (2016) 267–277, https://doi.org/10.1016/j.chembiol.2015.12.011.

[86] A. Zhou, et al., Synergistic interactions of vancomycin with different antibiotics against Escherichia coli: Trimethoprim and Nitrofurantoin display Strong Synergies with vancomycin against Wild-Type E. coli, Antimicrob. Agents Chemother. 59 (1) (2015) 276–281, https://doi.org/10.1128/aac.03502-14.

[87] B.C. Dalton, et al., Bacterial reduction with nickel-titanium rotary instrumentation, J. Endod. 24 (11) (1998) 763–767, https://doi.org/10.1016/S0099-2399(98)80170-2.

[88] V.C. Dinca, et al., Nickel–titanium alloy: Cytotoxicity evaluation on microorganism culture, Appl. Surf. Sci. 252 (13) (2006) 4619–4624, https://doi.org/10.1016/j.apsusc.2005.07.093.

[89] N. Ohtsu, S. Suginishi, M. Hirano, Antibacterial effect of nickel-titanium alloy owing to nickel ion release, Appl. Surf. Sci. 405 (2017) 215–219, https://doi.org/10.1016/j.apsusc.2017.02.037.

[90] A.R. Mhaske, et al., Antiadherent and antibacterial properties of stainless steel and NiTi orthodontic wires coated with silver against Lactobacillus acidophilus—an in vitro study, Prog. Orthod. 16 (1) (2015) 40, https://doi.org/10.1186/s40510-015-0110-0.

[91] H. Zhang, et al., Vancomycin-loaded titanium coatings with an interconnected micro-patterned structure for prophylaxis of infections: an in vivo study, RSC Adv. 8 (17) (2018) 9223–9231, https://doi.org/10.1039/C7RA12347G.

[92] S.R. Nodzo, et al., Cathodic voltage-controlled Electrical Stimulation plus prolonged vancomycin Reduce bacterial Burden of a titanium implant-associated infection in a Rodent model, Clin. Orthop. Relat. Res. 474 (7) (2016) 1668–1675, https://doi.org/10.1007/s11999-016-4705-7.